

## ABSTRACT

Title of Thesis: A MODEL OF THE AVIAN SUPERIOR OLIVARY  
NUCLEUS

Degree candidate: Raul Rodriguez Esteban

Degree and year: Master of Science, 2002

Thesis directed by: Professor Jonathan Z. Simon  
Department of Electrical Engineering

A computational model of the superior olivary nucleus (SON) was added to a model of the nucleus laminaris (NL) using the NEURON simulation language. The SON is an auditory nucleus situated in the ventrolateral region of the avian brainstem. It receives inputs from the ipsilateral nucleus laminaris (NL) and nucleus angularis (NA), and it projects back to the ipsilateral NL, NA and nucleus magnocellularis (NM). Its function is suggested to be inhibitory, controlling the size and precision of the spikes in the NL and the NM. However, the role it plays as a center of convergent input and divergent output is unknown. Our simulation shows how the SON improves the coincidence detection in the NL in different ways. First, the discrimination is increased because both coincidence detection spikes and erroneous spikes are reduced evenly, improving thus the ratio when the former outnumber the latter. Second, unilateral summation errors decrease because the inhibition helps differentiating these errors from binaural coincidence. The degree of heterogeneity of the SON cells leads us to hypothesize that it implies a specialization for the different kinds of inputs they receive.

A MODEL OF THE AVIAN SUPERIOR OLIVARY NUCLEUS

by

Raul Rodriguez Esteban

Thesis submitted to the Faculty of the Graduate School of the  
University of Maryland, College Park in partial fulfillment  
of the requirements for the degree of  
Master of Science  
2002

Advisory Committee:

Professor Jonathan Z. Simon  
Professor Timothy Horiuchi  
Professor Shihab A. Shamma



## ACKNOWLEDGEMENTS

I would like to thank Jonathan Simon for the confidence he put in me for this project. I would like to thank Kate Macleod for making the recordings we needed. I would like to thank also the advice of Sridhar Kalluri, Michael Burger and Nichola O'Hara.

## TABLE OF CONTENTS

List of tables.....	iv
List of figures.....	v
List of abbreviations.....	vii
Objectives of the model.....	1
CHAPTER I: Background & Significance.....	2
Sound localization in avians.....	3
Sound pathway for localization.....	4
The nucleus laminaris.....	7
The CD Model.....	10
Flaws in the CD model. Reasons to incorporate a SON.....	13
Historical studies of the SON.....	14
Discussion of the role of the SON.....	18
CHAPTER II: Methods.....	23
Theoretical background of the model.....	24
The Rall approach.....	24
The Hodgkin and Huxley description of the squid giant axon.....	26
Model proposal.....	27
The NEURON language simulation approach.....	29
Conceptual implementation of the model by NEURON.....	30
Data from Katrina Macleod.....	32
CHAPTER III: Results.....	33
Parameters & actual implementation of the model.....	34
Parameters found empirically.....	43
Synaptic connections.....	46
The CD+SON model performance.....	52
Assessment of the input of the SON.....	62
Bibliography.....	73

## LIST OF TABLES

Table 1. Average and st. dev. of the ball-and-stick model parameters in a SON cell.	35
Table 2. Degree of approximation of the model to the empirical recordings.	45
Table 3. Parameters of the SON model.	71

## LIST OF FIGURES

Figure 1. ITD as an indicator of the azimuthal direction of a sound source.	4
Figure 2. Left: definition of contralateral and ipsilateral sides. Right: section of the chicken nervous system with the location of the auditory nuclei of the brainstem (after Soares et al. (2002)).	5
Figure 3. Example of phase locking. Spikes are triggered when the signal is in a fixed phase.	6
Figure 4. Detail of the bilateral projections of the NM to the NL in chickens (after Kubke and Carr (2000)).	7
Figure 5. Left: the Jeffress model of coincidence detection (after Jeffress (1948)). Right: the Jeffress model applied to the NM projections to NL (after Overholt et al. (1992)).	8
Figure 6. Fibers from NM branching in NL. The scale bar represents 1 mm (after Carr and Konishi (1990)).	10
Figure 7. The inhibition as implemented originally in the CD model. The red dot represents the integration of spikes (after Simon et al. (2001b)).	14
Figure 8. Auditory nuclei of the chicken brainstem and connectivity of the SON (after Yang et al. (1999)).	16
Figure 9. Conceptual design of the model by Pena et al. (1996).	19
Figure 10. Left: decomposition of a dendritic arbor in segments (after Rall (1959)). Right: the ball-and-stick model (after Johnston and Wu (1995)).	25
Figure 11. Model of the active behavior of the neuron membrane (after Hodgkin and Huxley (1952)).	27
Figure 12. Left: a typical SON cell (after Yang et al. (1999)). Right: a generic model for stellate cells (after Banks and Sachs (1991)).	28
Figure 14. SON cell current injection response curves in Yang et al. (1999).	32
Figure 17. Set of curves s3.	43
Figure 18. Set of curves of the SON model.	46

Figure 19. Simulation of a postsynaptic response in a SON cell after excitation with a current injection of 0.7 nA and 10 ms. The NL cell has a best frequency of 2000 Hz.	48
Figure 20. Typical postsynaptic recording of a NL cell while exciting extracellularly SON cells (after Yang et al. (1999)).	50
Figure 21. Simulation of a postsynaptic response in NL after injecting a current of 0.3 nA and 40 ms in a SON cell.	51
Figure 22. NL cell while being excited by a sound of 700 Hz and without SON inhibition.	57
Figure 23. NL cell with a sound of 700 Hz and the inhibition of 5 SON cells that are excited with a current injection of 0.6 nA.	58
Figure 24. Effect in a SON cell of a NL cell spiking with a sound of 700 Hz.	63
Figure 25. Effect in a SON cell of a NL cell spiking with a sound of 2000 Hz.	64
Figure 26. SON cell spiking fast (96 spikes/s) due to the input of the NA.	65
Figure 27. SON cell with a combined input from NA and a NL cell.	66
Figure 28. Panel of parameters of the SON model.	72

## LIST OF ABBREVIATIONS

0E	Unilaterally excited.
1-D	One dimensional.
2-D	Two dimensional.
3-D	Three dimensional.
8N	Cranial nerve VIII.
a.k.a.	Also known as.
$A_t$	Total area of the membrane cell.
CD	Coincidence detection.
$C_m$	Membrane capacitance.
DR	Discharge rate.
E	Resting potential.
$E_{Cl}$	Chlorine resting potential.
EE	Excitatory-excitatory, bilaterally excited.
GABA	Gamma-aminobutyric acid.
GABA-I	Gamma-aminobutyric acid immunoreactivity.
HH	Hodgkin and Huxley.
ILD	Interaural level difference.
IPSP	Inhibitory postsynaptic potential.
ITD	Interaural time difference.
$K^+$	Potassium ion.

l	Physical length.
L	Electrotonic length.
LNTB	Lateral nucleus of the trapezoid body.
LVA	Low voltage activation.
MNTB	Medial nucleus of the trapezoid body.
MSO	Medial superior olivary.
NA	Nucleus angularis.
Na <sup>-</sup>	Sodium ion.
NL	Nucleus laminaris.
NM	Nucleus magnocellularis.
PSP	Postsynaptic potential.
R <sub>N</sub>	Total cell input resistance.
R <sub>m</sub>	Membrane resistance.
s	Seconds.
SI	Synchronization index.
s-ITD	Simulated interaural time difference.
SON	Superior olivary nucleus.
SR	Spike rate.
St.Dev.	Standard deviation.
T	Signal period.
VS	Vector strength

## Objectives of the model

The main objective of the model has been to test the influence of the superior olivary nucleus (SON) in the process of sound localization in avians. In particular, we wanted to enhance a previous model of the nucleus laminaris (NL), which is the center of what has been called ‘coincidence detection’. Coincidence detection is the critical process that allows avians to localize sounds with respect to its azimuthal position. Since the NL receives an important input from the SON, we have been compelled to test its magnitude and variability.

The modeling scheme that we have constructed is a computational model based on standard modeling techniques of neuronal electrical behavior. The parameters for the simulation are adjusted to match published electrophysiological experiments. The computational power of the computer simulation allows us to observe in real time the way ionic currents change inside of the cell.

The secondary objective of the model is to analyze the role of the SON as a source of a multi-purpose output. The SON receives inputs from the NL and the nucleus angularis (NA), and sends its output to the nucleus magnocellularis (NM), NL and NA. The reasons for a multi-purpose function like this one are not well known.

Finally, the model tries to increase our understanding of the characteristics of the SON and how necessary is in the auditory processing of the avians.

This document has been intended also as a reference for future developers of the model.

CHAPTER I  
Background & Significance

## Sound localization in avians

The auditory system of avians performs sound localization using two cues: interaural level difference and interaural time difference.

The interaural level difference (ILD) is the difference of intensity between the sound received in one ear versus the other ear. The cause of this difference is the interaction of the incoming sound with the head and the body. The characteristics of this interaction can be summarized in a function called HRTF (Head Related Transfer Function). For example, in the barn owl (*Tyto Alba*), the right ear is pointing up and the left ear is pointing down. Therefore, a sound coming from above is received louder in the right ear, and conversely. In other birds there is no evidence that ILDs are the basic cue for elevation detection and it seems likely that it depends more in characteristics of the specific HRTF of the animal.

The interaural time difference (ITD) is the time difference between the arrival of a sound to an ear and its arrival to the other. A sound that is originated equidistantly to the ears arrives at the same time to both ears, but a sound that is skewed to the side arrives first to the ear that is nearer.

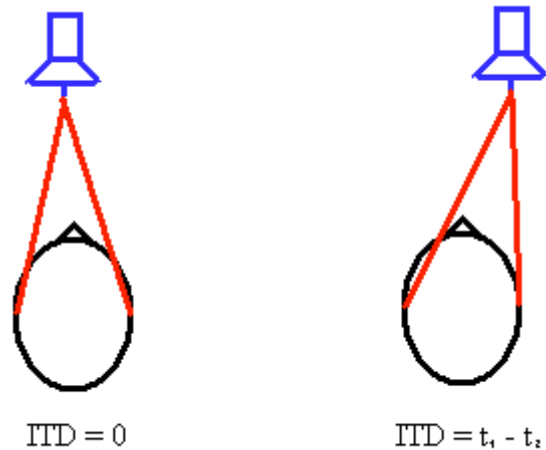


Figure 1. ITD as an indicator of the azimuthal direction of a sound source.

Processing the ITD and the ILD of a sound conveys information to the animal about the direction towards which the sound originated. The ITD gives information about the azimuth (direction in the horizontal plane) and the ILD about elevation (direction in the vertical plane), and both combined help the animal to map the surrounding auditory space (for a review see Carew (2000)).

### Sound pathway for localization

In avians, the pathway for sound localization involves two processing branches. After the sound is received at the pinna it goes down the ear canal and is processed in the cochlea. The cochlea has in its tube a set of hair cells. Each of these hair cells vibrate with a sound corresponding to a narrow frequency band and transduces this vibration into an electrical signal. The combined action of the hair cells, in fact, parcels in channels a part of the frequency band that arrives to the cochlea. The size of this band is different in every avian.

The electrical signals created in the cochlea, which is part of the inner ear, are then sent in two directions (via the cranial nerve VIII (8N)): to the nucleus angularis (NA) and to the nucleus magnocellularis (NM). These nuclei, i.e. groups of neurons, are called primary nuclei (Boord, 1969) and they are located in the brainstem.

The 8N of an ear serves the NM and NA of its side of the brainstem, existing both in each side of the brainstem. In order to differentiate the nuclei of one side from the nuclei on the other side we call ipsilateral nuclei those that are on the side where the primary input comes from. The nuclei on the other side are called contralateral. E.g., if we are studying the sound coming from the left ear then the ipsilateral NM and NA are those in the left side of the brainstem, while the contralateral are those in the right side.

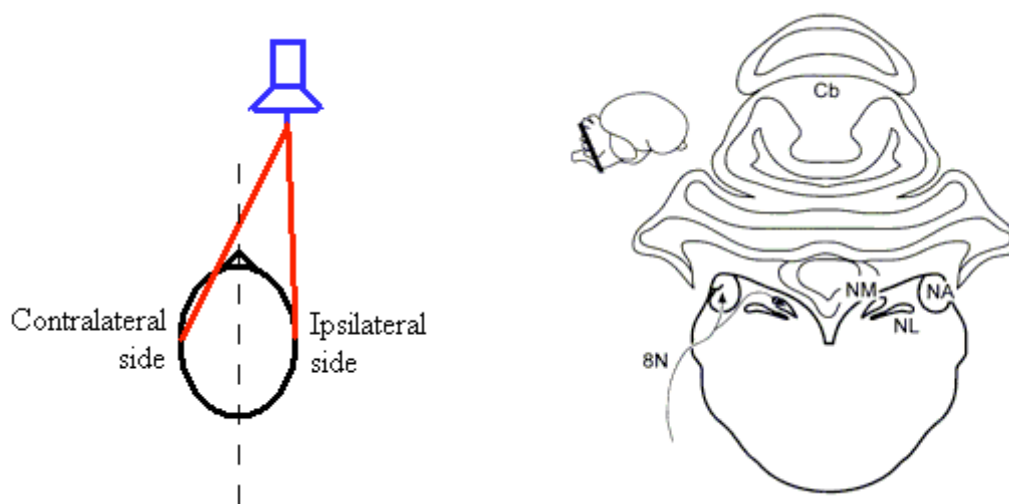


Figure 2. Left: definition of contralateral and ipsilateral sides. Right: section of the chicken nervous system with the location of the auditory nuclei of the brainstem (after Soares et al. (2002)).

The NM pathway is believed to be involved in ITD processing and is the main source of azimuthal information. The NA pathway is involved more in ILD than in ITD processing

(Sullivan and Konishi, 1984). While the role of the NM is accepted to be ITD processing, the role of the NA seems to be more heterogeneous (Warchol and Dallos, 1990; Soares et al., 2002).

NM cells fire spikes at a particular phase of the incoming signal, producing a phenomenon called phase locking (Sullivan and Konishi, 1984). This kind of cell is called “primary-like”. A NM cell may not be able to fire every time the incoming signal is at a particular phase, especially at high frequencies, but it fires consistently *only* at that phase.

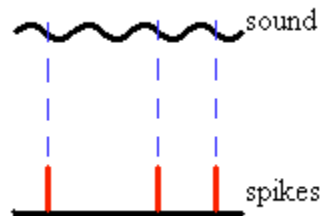


Figure 3. Example of phase locking. Spikes are triggered when the signal is in a fixed phase.

Within the NM cells are arranged tonotopically; that is, the cells are arranged with regard to the frequency (the tone) at which they fire best (Young and Rubel, 1983). The cells are arranged with regard to the frequency (the tone) at which they fire best. E.g., low frequency cells are on one side of the NM and high frequency cells are on the other. This organization, for example, covers a range between 500Hz and 4100Hz in chickens (Rubel and Parks, 1975).

Low frequency information coming from the 8N is maintained after passing the NM. The phase locking in the NM cells maintains all the low frequency information (Reyes et al., 1996).

## The nucleus laminaris

The NM cells project both to the contralateral and the ipsilateral nuclei laminaris (NL) (Parks and Rubel, 1975), which are called secondary nuclei. NL cells have two main dendritic arbors and each arbor receives input from only one NM. The input from the ipsilateral NM comes from the dorsal direction and the input from the contralateral NM comes from the ventral direction. Each one of these inputs goes across separated dendritic arbors and flows into the soma of the NL cell. Thus, the inputs to the NL cells are bilateral and segregated spatially.

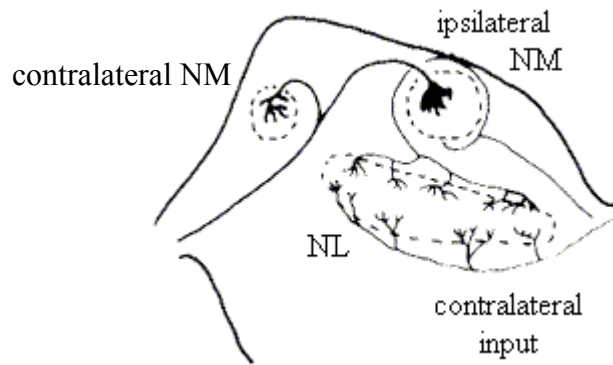


Figure 4. Detail of the bilateral projections of the NM to the NL in chickens (after Kubke and Carr (2000)).

Cells in the NL are also arranged tonotopically, seemingly in the same order as they are in the NM (Rubel and Parks, 1975). This tonotopic distribution in the NL entails a related anatomical variation. NL cells on the high frequency extreme have a large number of very short dendrites. The dimensions and size of the dendrites decrease linearly along the frequency axis. In the low frequency extreme, cells bear a small number of very long dendrites (Smith and Rubel, 1979).

The NM projections to the NL are also distributed following the same axis. Fibers coming from the NM associated with high frequencies are connected to NL cells that fire at high frequency, and conversely (Young and Rubel, 1983).

The actual function of the NL is suggested to be the comparison of phase differences between the sounds arriving to each ear (Carr and Konishi, 1990; Overholt et al., 1992; Pena et al., 2001). This phase difference represents the difference in the distance traveled by the sound. A sound nearer to an ear (the ipsilateral ear) travels a shorter distance and arrives with a different phase to that ear than to the other ear. The model used to explain how this happens is known as the Jeffress model, or the coincidence detection model (Jeffress, 1948).

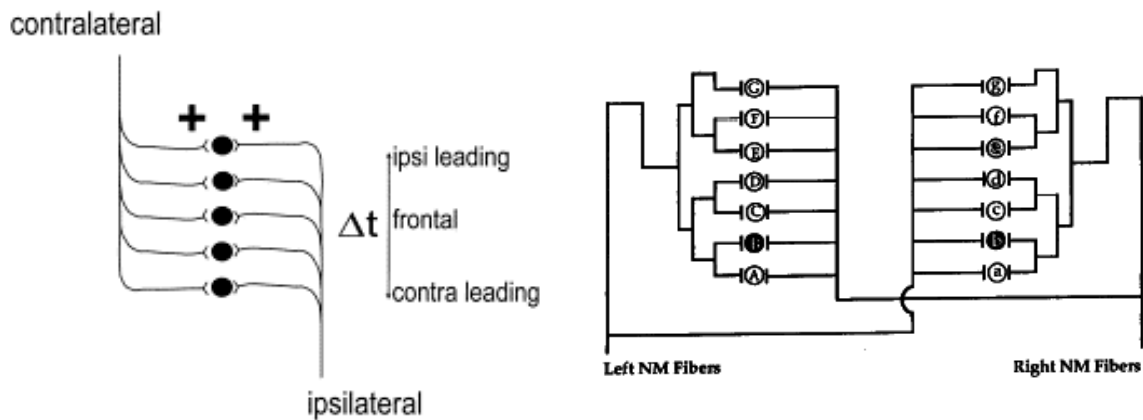


Figure 5. Left: the Jeffress model of coincidence detection (after Jeffress (1948)). Right: the Jeffress model applied to the NM projections to NL (after Overholt et al. (1992)).

The fibers coming from both NM branch heavily around the NL cells. This branching is laid out in a determined pattern. When the signal arrives at the tip of every branch it has gone through a given distance. Every signal in a branch is going to arrive sooner or later depending on how long it is their pathway.

This branching is progressively longer for the fibers coming from the contralateral side (Carr and Konishi, 1988). Pathways are increasingly longer following an axis. According to the Jeffress model, this situation is exploited to compute ITDs. The NL cells would perform the task of coincidence detection. This means that they fire only when their inputs arrive at the same time (or in a window of time).

Since the pathways are arranged purposefully, the signal arrives with different delays to every NL cell. A conveniently disposed group of NL cells is able to 'detect' a useful range of delay differences.

The NL cells that have a shorter left afferent detect sounds coming from the right side. Thus, the extra pathway compensates the time advantage of the right side. If a NL cell has afferents of similar length, it fires when the sound arrives at the same time to both ears.

A number of coincidence detection (NL) cells with inputs that travel adequate distances is able to perform the task of computing ITDs. The delay difference is encoded within the firing of the NL cells. A cell firing within its group *signals* the azimuthal direction from which the sound is coming (Carr and Konishi, 1990; Overholt et al., 1992).



Figure 6. Fibers from NM branching in NL. The scale bar represents 1 mm (after Carr and Konishi (1990)).

Inside this conceptual framework given by the Jeffress model it is important to stress the frequency aspect. High frequency cells have small dendritic arbors. In general, dendritic arbors are assumed to have mostly a passive behavior: they conduct and sum incoming signals adding some delay and smoothing. Thus, small dendritic arbors have smaller response time windows because the incoming signals flow through them in a short time. This response time window entails a given preferred interstimulus time interval. The interstimulus time interval is the time difference between the arrivals of two sequential stimuli. The fact that the cell can act quicker because of the short dendrites enables it to fire optimally with inputs that come within small periods. On the other hand, large dendritic arbors have longer latency periods and therefore have longer response time windows and larger optimal interstimulus arrival time.

#### The CD Model

The Coincidence Detection (CD) model (Simon et al., 1999; Simon et al., 2001a; Simon et al., 2001b) is an electrical model that tries to reproduce the *in vivo* electric flow inside

NL cells. Even with state-of-the-art techniques, *in vivo* (with the animal alive) intracellular recordings of NL cells are very difficult<sup>1</sup>. Thus, a model of these cells becomes necessary to test a number of hypotheses about the coincidence detection mechanism.

The conceptual layout of the model exploits mainly the spatial segregation of inputs. It creates an array of NL cells, each cell with a soma, an axon and dendrites. The soma is connected to a number of dendrites attached to each side. The axon is connected to one side of the soma. The dendrites vary in size and number depending on the optimal frequency at which the NL cell fires best – as it happens in real NL cells (Smith and Rubel, 1979).

The input to the NL cell is created simulating synapses coming from the NM. These synapses are spread along the dendrites. The nature of their activation is related to the phase-locking behavior of the NM cells. Given a sound source with a fixed frequency (a pure tone), the synapses fire in a phase locking fashion: always at the same phase of the tone, mimicking real NM cell firing. The accuracy of this phase locking can be changed to emulate different animals. E.g. owls perform better phase locking than chickens (Warchol and Dallos, 1990; for a review, Kubke and Carr (2000)).

The actual implementation of the NL cell is based on two sets of ideas of electrical modeling of neurons. One is the modeling of the passive electrical behavior of neurons by Rall. The other is the modeling of active channels in neurons by Hodgkin and Huxley (HH model). These ideas will be discussed later since they are also used in the SON model.

---

<sup>1</sup> But not impossible, see Carr and Konishi (1990).

What is most characteristic of the CD model is that, unlike the HH model, NL cells use two potassium (K) channels, one of unusually rapid activation (rapid response) and one of slower activation (slower response). This was found in a study by Parameshwaran et al. (2001), and is further discussed in Simon et al. (2001a).

The main parameters that monitor the performance of the CD model are: (a) vector strength, (b) interaural time difference (ITD) discrimination, and (c) spike rate.

(a) Vector strength (VS) or synchronization index (SI) (Goldberg and Brown, 1969).

The vector strength is a measure that can be used to compare the degree of phase locking of a process. In particular we are interested in knowing to what degree the phase locking is lost, or gained, in the NL cell processing. The VS is calculated this way:

$$VS = \frac{1}{N} \sqrt{\sum_i \cos^2 \phi_i + \sum_i \sin^2 \phi_i}$$

$$\phi_i = 2\pi \frac{\text{mod}(t_i, T)}{T}$$

Where  $t_i$  is the time of arrival of a spike,  $T$  is the period of the original sound and  $N$  is the total number of spikes. The VS measures how spikes fit to a given periodicity. When a spike is fired consistently at a given phase  $\phi_i$  the vector strength is 1.

(b) ITD discrimination.

It is the ratio between the spikes that produces a neuron firing maximally and a neuron firing minimally. A NL neuron that is firing maximally is one that receives inputs at the same time. We say of these neurons that they receive inputs ‘in-phase’ because the signals (that were originally tones before being phase-locked at the NM) are arriving with

the same phase. A NL neuron that receives its inputs in counter phase fires minimally.

This means that when the input of one side is arriving with maximum intensity the input of the other side is arriving with null intensity.

Since the ITD discrimination is a ratio, a very low minimal firing rate can distort its interpretation. Alternatively, it can be defined as  $1 - (r_{\min}/r_{\max})$ , where  $r_{\min}$  is the minimal firing rate and  $r_{\max}$  is the maximal firing rate.

(c) Spike rate (SR) or discharge rate (DR).

Another measure of good performance of a NL cell is its spike rate. When the NL cell is firing maximally it should spike at around 100-500 spikes per second (Reyes et al., 1996). When it is firing minimally it should spike at a lower or equal value, it depends on the frequency of the source. At low frequencies the SR is near 0, and at high frequencies is close to or at the maximally firing rate. Generally, the average SR varies across animals.

### Flaws in the CD model. Reasons to incorporate a SON

The CD model performs poorly at high frequencies. For a CD model of the chicken, the ITD discrimination is poor at 1400Hz, and an overflow of current appears at higher frequencies such as 2000Hz. Given that the chicken can still localize sounds at those frequencies an enhancement of the model is needed.

A way of doing this is to add a simple inhibitory input to the NL cell, since physiological studies point out the existence of inhibitory synaptic terminals in the NL. These terminals have a neurotransmitter called  $\gamma$ -aminobutyric acid (GABA) (Code et al., 1989; Carr et al., 1989; von Bartheld et al., 1989). To model them, a spike integration process was

added. The integration consists in counting a fixed number of spikes. After the spikes are counted the integrator triggers an inhibitory PSP<sup>2</sup>.

This inhibition fails to improve the coincidence detection. It seemed that the inhibitory PSPs (IPSPs) were ineffective because they came randomly with respect to the timing of the ITDs. The inhibition simply leveled the electrical flow in the NL cells. A further step to increase the complexity of the inhibition was then taken creating a model of the source of the inhibition, the superior olivary nucleus (SON).

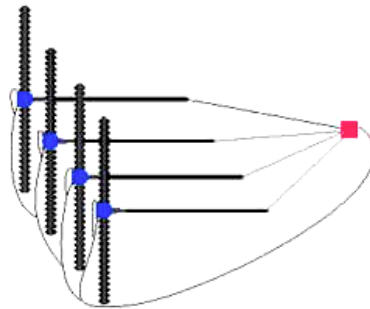


Figure 7. The inhibition as implemented originally in the CD model. The red dot represents the integration of spikes (after Simon et al. (2001b)).

### Historical studies of the SON

The presence of inhibition in the NL was recognized early. NL cells show immunoreactivity when an antiserum to GABA is used, a phenomenon called GABA-immunoreactivity (GABA-I). GABA is a substance present in high concentrations in the central nervous system. It is supposed to mediate the action of inhibitory synapses

---

<sup>2</sup> This integrative behavior is suggested in Yang et al. (1999) by observing the response to PSPs of the SON cells.

because its release mediates the opening of chlorine (Cl<sup>-</sup>) ionic gates<sup>3</sup>. High concentrations of GABA indicate the possible existence of inhibitory inputs (Kandel and Schwartz, 1989).

Code et al. (1989) described the appearance of GABAergic neural terminals in the embryo of the chicken. The first sign of GABA-I is in embryonic day 12 (chickens hatch in 21 days) and it peaks in post-hatch chickens.

The source of these inhibitory terminals was not clear then, and for the most part they were attributed (von Bartheld et al., 1989) to cells situated locally in the surrounding neuropil of the NM and the NL. More specifically, they came from a group of cells between the NM and the NL that were described previously by Muller (1987) and Carr et al. (1989). Later, it was discussed that such a small population of cells was unlikely to generate the dense number of GABAergic terminals that were found in NL, and that the SON was the likely origin of most of them. With a series of experiments they found out that descending fibers from the SON matched the distribution of the GABAergic terminals (Lachica et al., 1994).

The SON is one of the four auditory nuclei of the avian brainstem (being the four: NA, NM, NL and SON). It receives input in its medial side from the ipsilateral NL and in all parts from the ipsilateral NA (Conlee and Parks, 1986; Takahashi and Konishi, 1988). It projects back to the ipsilateral NM, NL and NA (Lachica et al., 1994). Lachica et al. (1994) proposed that it also projected to the contralateral NM, NL and NA; but this was refuted later (Yang et al., 1999; Monsivais et al., 2000).

---

<sup>3</sup> More on membrane gates will be discussed later in the Hodgkin and Huxley model.

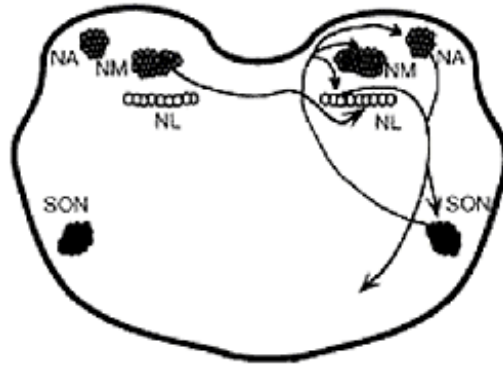


Figure 8. Auditory nuclei of the chicken brainstem and connectivity of the SON (after Yang et al. (1999)).

The function attributable to the SON was not clear in the beginning. There appeared to be different types of cells in the SON. This fed the idea that the SON may be doing a number of different functions. Takahashi and Konishi (1988) described two categories of cells in the SON: EE (excitatory-excitatory) cells, which respond to bilateral cues such as ITDs or ILDs; and OE cells, which respond to unilateral sounds. They attributed to the OE cells the processing of the input from the NA, and to the EE cells the processing of bilateral inputs from both NA<sup>4</sup>. Alternatively, they hypothesized that the cells might be processing ITD information coming from the NL.

Carr et al. (1989) described two types of SON cells: large multipolar cells, which are similar to those in NM, and medium-sized, fusiform cells.

Lachica et al. (1994) performed a deeper physiological analysis of the SON cells and arrived at similar conclusions. They reported that some cells fire with pure tones, others react with the phase, and others are not active at all. It appeared that some SON cells are more suitable to NL input than others, while the others are more suitable to NA input.

---

<sup>4</sup> The inputs of SON were not known.

However, it seemed clear that most SON cells were GABAergic in nature, about a 70% of them (Lachica et al., 1994), and that the NA had a bigger projection to the SON than the NL (Takahashi and Konishi, 1988; Lachica et al., 1994).

Once accepted that the inhibition in NL and NM comes from the SON, the focus of investigation shifted to the effects of this inhibition (Hyson et al., 1995; Hyson and Sadler, 1997; Bruckner and Hyson, 1998; Funabiki et al., 1998; Lu and Trussell, 2000). Funabiki et al. (1998) found that inhibition in the NL is mediated by GABA<sub>A</sub> receptors (for a review of types of GABA, Chehib and Johnston (1999)), which activate Cl<sup>-</sup> channels. An opposing view was suggested by Hyson et al. (1995). He proposed that the inhibition was mediated by a special GABA receptor, possibly a variant of the GABA<sub>A</sub> receptor. This was refuted later by Yang et al. (1999).

Funabiki et al. (1998) also analyzed the characteristics of the inhibitory PSPs (while assuming they were coming from the SON). These spikes have fast rising time and slow decaying time. They also hypothesized that, given the chlorine resting potential ( $E_{Cl}$ ) observed, *in vivo* IPSPs would probably be depolarizing. Unlike other commoner IPSPs, these would increase the voltage in the cell (for more details see below, and also Monsivais and Rubel (2001)).

Hence, they postulated that the inhibition improved the coincidence detection by decreasing the cell's time constant<sup>5</sup>. NL cells that received a simulated steady GABAergic input presented smaller, sharpened and more precise spikes.

---

<sup>5</sup> Since the time constant of the cell ( $\tau$ ) is the product of its total input resistance ( $R_N$ ) and the membrane capacitance ( $C_m$ ):  $\tau = R_N C_m$

Then, increasing the total conductance ( $g_N = 1/R_N$ ) decreases the time constant ( $\tau$ ) which means the cells has a faster response and is thus more precise.

Yang et al. (1999) undertook an electro physiological study of SON cells. Unlike other studies, they stated that the SON cells have a high degree of homogeneity with regard to their morphological and firing properties. Their affirmation has to be taken cautiously since they did not do a large survey of cells<sup>6</sup> (n=23). They also described their behavior as being roughly integrative, with temporal summation of inputs before firing. The IPSPs that the SON triggers in NL were described as having a fast rise and a slow decay, as in Funabiki et al. (1998). They also suggested that part of the reduction of the input resistance is due to the recruitment of LVA K<sup>+</sup> channels (ionic potassium channels that are opened at low voltage levels). Thus, inhibition not only increases conductance, but also inactivates channels that are necessary to create spikes such as sodium and low voltage potassium channels.

Moreover, studies in NM show that the conductivity increase inactivates Na<sup>+</sup> channels, effectively slowing the spike firing process (Koyano et al., 1996; Lu and Trussell, 2001).

### Discussion of the role of the SON

The previously discussed studies give a framework from which the influence of the SON in the NL can be assessed and modeled. An example of a model of the SON has been published by Pena et al. (1996). They compared physiological recordings of NL cells with a modeled version of NL that had only NM input. They argued that NL neurons receive a large input from NM, between 45 and 150 afferent fibers (Carr and Boudreau, 1993), while NM neurons fire at increasingly higher rates with higher sound intensity. At a certain point, NL neurons in their model saturate, and the first ones to saturate are the

---

<sup>6</sup> Suggestion of Michael Burger, from the University of Washington.

ones that fire maximally: in-phase neurons. Meanwhile, out-of-phase neurons continue increasing their firing rates with the intensity. If the input to NL is high enough, all NL cells saturate equally and fire at the same rate.

While their model performed poorly with high sound intensity levels, the actual recordings in the NL did not. Therefore, they hypothesized that inhibition had a role in modulating threshold crossing<sup>7</sup> and they constructed a modified model adding SON.

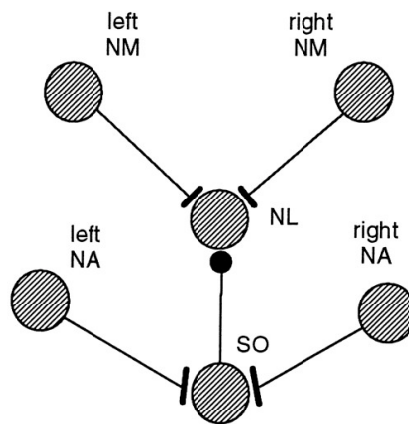


Figure 9. Conceptual design of the model by Pena et al. (1996).

This model effectively improved the coincidence detection at high sound levels. Viète et al. (1997) proved further this point.

Unlike our model<sup>8</sup>, Pena et al. (1996) did not include input from the NL to the SON. This is mainly because they were interested in high sound intensity performance and not in frequency performance.

---

<sup>7</sup> Threshold crossing is the indicator of coincidence detection. When a spike in the axon tip of the NM cell surpasses the threshold coincidence detection is declared. Moving the threshold up or down respectively hinders or facilitates coincidence detection.

<sup>8</sup> More details about our model are discussed later.

Before starting to discuss our model we would like to show two other inhibitory systems that resemble the one we are interested in: (a) the SON inhibition on NM, and (b) the inhibition on the mammal NL homolog, the medial superior olive (MSO).

(a) The SON inhibition on NM.

The SON inhibition in NM has been characterized in a similar way as it has been in the NL: slow GABAergic depolarizing IPSPs recruit LVA  $K^+$  channels and inactivate  $Na^+$  channels (Monsivais et al., 2000; Lu and Trussell, 2001; Monsivais and Rubel, 2001).

The conclusion that can be drawn from this picture is that the goal of the inhibitory mechanism is similar in both NL and NM: improve the temporal precision and reduce the high spiking rate. The NL input to the SON would be the indicator of a high spiking rate.

The fact that the SON only projects back to the ipsilateral NM avoids that an excessive sound loudness from an ear distorts the coincidence detection (Hyson et al., 1994; Monsivais et al., 2000). On the other hand, Lachica et al. (1994) proposed that the SON introduces a bilateral regulation in the otherwise unilateral NM and NA processing. Since the SON receives bilateral information from the NL, it seems possible that it influences the NM and NA processing. This possibility was refuted partially by Viète et al. (1997). They showed that high sound intensity in an ear did not drive up the spiking rate of the contralateral NM. It has yet to be proved that the same happens with respect to frequency variations.

The function of the NA input to the SON, and its feedback, is still not well understood.

The NA has been usually known for his involvement in sound intensity processing (Takahashi et al., 1984; Sullivan and Konishi, 1984). Nonetheless, NA cells have been

described recently as being of at least 3 electrical classes: with tonic firing, with decaying firing and one-spike (Soares and Carr, 2001; Soares et al., 2002). The NA also has a tonotopic distribution (Koppl, 2001). The function that the SON may have in NA processing is still not known.

Since the SON is a center of convergent inputs and divergent outputs we hypothesize that the SON may perform a function that is equally useful to different nuclei. High intensity levels saturate NL neurons (Pena et al., 1996). The SON acts on the NL and on its source, the NM, to solve this problem. However, at the same time it projects to NA, indicating that it may have some role regulating tonic firing in NA cells.

Similarly, the NL may activate the SON for frequency related reasons. In this case the SON input from NA may indicate that there is NA cells that have frequency related problems as well. For example a high frequency may drive an inhibitory output from the SON that would influence the NA.

#### (b) Inhibition in the MSO

The MSO is regarded as the mammalian counterpart to the NL (Boord, 1969; Takahashi and Konishi, 1988). Its processing follows roughly the Jeffress model (Yin and Chan, 1990). However, the processing of ITDs itself seems to involve different biological mechanisms in mammals than in avians (for a review: Grothe, 2000). Also, the MSO appears to have other functions in some mammals of small body. For our purposes, it is remarkable that the inhibition is driven by two nuclei, the medial and lateral nucleus of the trapezoid body (MNTB and LNTB), which produce a very precise inhibition (Brand

et al., 2002). Thus, it presents an alternative way of doing the task that the SON performs. Unfortunately, little is known about how this inhibition works.

CHAPTER II  
Methods

## Theoretical background of the model

The construction of our model is based on two major modeling contributions:

- (a) The mathematical modeling of the passive electrical behavior of neurons by Rall (for a review: Rall, 1995).
- (b) The neural membrane channel characterization by Hodgkin and Huxley (Hodgkin and Huxley, 1952; for a review: Johnston and Wu, 1995).

### The Rall approach

Rall (1959) proposed that a neural dendritic tree could be simplified with regard to its electrical properties. Assuming that dendrites behave like passive cables (metallic cylinders) and other homogeneity assumptions (see Appendix A), he proposed a method to simplify complex dendritic arbors. Thus, a dendritic arbor could be analyzed as a simple cable as far as only its output response was studied.

The rationale he used is roughly as follows: a dendritic segment starting at the soma connects with other segments. These connections do not have reflections and hence they behave like cables with no ‘sealed’ end. Or, in mathematical terms, they are like infinite cables because they do not have reflections. After this, we assume continuity between the different cable segments. The current that has to flow between a cable segment and its output branches has to be the same. We apply conservation of electrical flow at every junction.

By applying these two ideas (conservation of electrical flow and assuming that every segment is ‘infinite’) we can elucidate the output characteristics of the total dendritic tree as it is seen from the soma. The problem gets reduced to a collation of different electrical

tubes. More importantly, the output characteristics of the arbor can be then redefined as the characteristics of a single cable.

Later, Rall (1960) showed that the response of a neuron to a current injection in the soma could be divided into two separable contributions: the contribution of the soma and the contribution of the dendrites. He argued that each contribution corresponded to an exponential function. Analyzing them separately it was possible to define the electrical characteristics of the soma and the dendritic arbor. Then, these characteristics could be used in a simple model: the ball-and-stick model (a.k.a. model of finite cylinder with lumped soma).

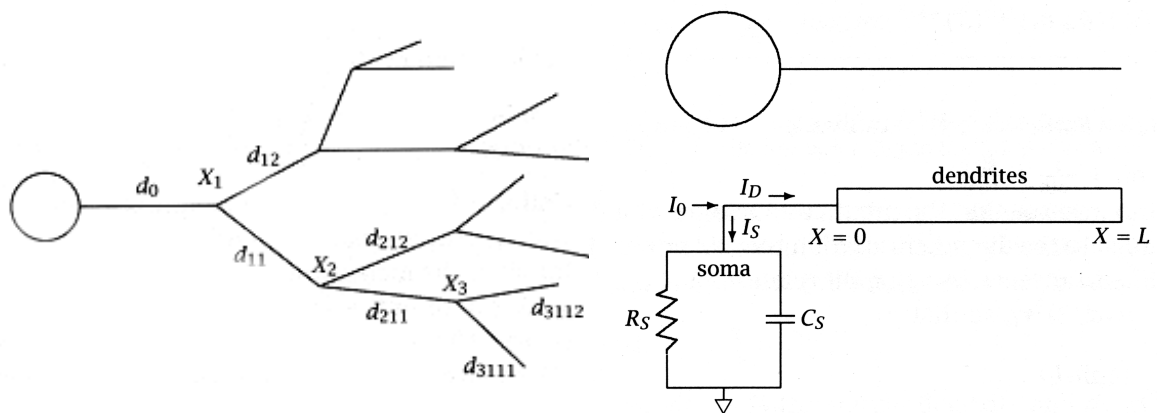


Figure 10. Left: decomposition of a dendritic arbor in segments (after Rall (1959)). Right: the ball-and-stick model (after Johnston and Wu (1995)).

This model, in its simplicity, loses the ability to simulate a variety of spatial configurations that a neuron may present. Rall proposed a way to overcome this limitation without over burdening the computational cost of a simulation. He proposed to divide the cell in electrical compartments (Rall, 1964). Every part of the neuron can be reduced to a piece of cable. This piece of cable can be subdivided in smaller pieces.

Morphologically complex neurons can be then approached. A numerous enough set of

cable pieces well arranged can approximate the original neuron. In the limit, compartments of differential sizes can simulate any neuron.

The compartmental approach also relaxes the original assumptions needed for the ball-and-stick model, since we are allowed to describe every piece of cable separately.

### The Hodgkin and Huxley description of the squid giant axon.

Hodgkin and Huxley (1952) summarized their findings while recording the squid giant axon with the voltage clamp technique. While the Rall models involve passive mechanisms of electrical flow (such as the cable equation) Hodgkin and Huxley described the way in which the neuron can dynamically influence the current flow. They proposed an electrical model that mimicked the spike (a.k.a. action potential) generation in the neuron. They parameterized the contribution of sodium ions ( $\text{Na}^+$ ) and potassium ions ( $\text{K}^+$ ) to this generation.

Sodium and potassium ions play a dynamic role in the neuron by means of ion channels situated in its membrane. These channels are proteins that regulate the flow of these ions in and out of the cell. These transmembrane proteins open and close depending of the intracellular voltage. Thus, they are called voltage-gated ion channels. Their properties are complex to explain. Hodgkin and Huxley tried instead describing them phenomenologically by fitting their data.

There are other ways in which ions cross in and out of the membrane; the most important through the leakage. This is controlled by proteins that are always 'open'. Joining together active and passive channels they were able to describe how a spike is created in the squid giant axon.

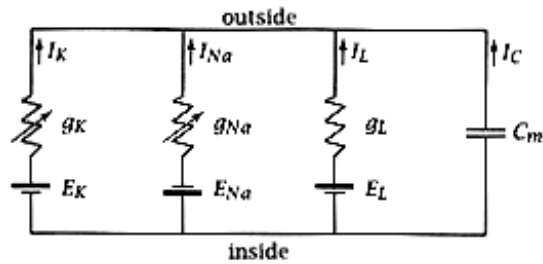


Figure 11. Model of the active behavior of the neuron membrane (after Hodgkin and Huxley (1952)).

What is most interesting in this model is that it has an ample amount of hand-tuned parameters. These can be “tweaked” to simulate potassium and sodium channels of other neurons, and also other types of channels.

#### Model proposal

Our model proposal follows the modeling fundamentals discussed below. A SON cell is created with three main parts: dendrites, soma and axon. Every part is divided into the number of compartments suitable for the model. The physiological data necessary to construct the model is taken mainly from Yang et al. (1999). They described the SON cells as being stellate (chopper) cells with at least 3 dendrites.

Our morphological construction of the cell follows the guidelines of a stellate cell model by Banks and Sachs (1991). In this model they propose a cell with 6 dendrites with 10 compartments each, a soma with 1 compartment, and an axon with 1 compartment.

The dendrites are passive – they do not have active channels. In the soma and in the axon there are channels of the Hodgkin and Huxley (HH) type.

A later model, White et al. (1994), shows an application of the ball-and-stick paradigm that simplifies the Banks and Sachs (1991) analysis. Applying the White et al. (1994)

method with Yang et al. (1999) electrophysiological data we could fully characterize the passive behavior of our model.

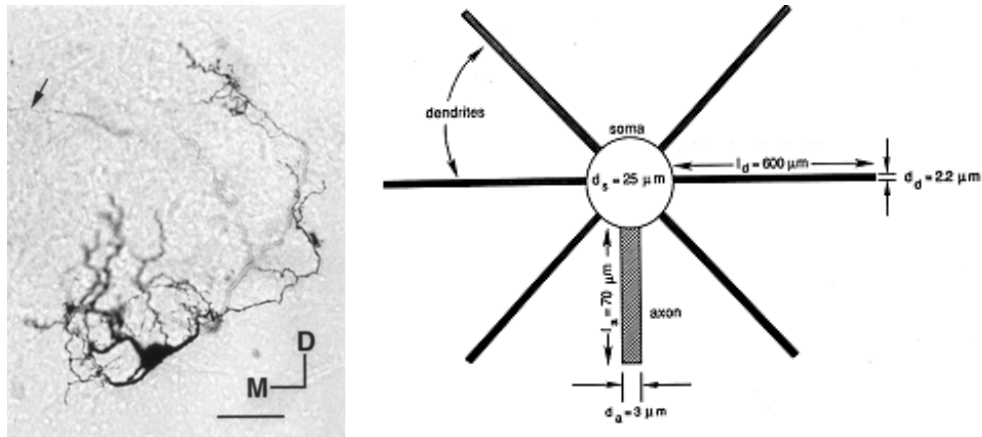


Figure 12. Left: a typical SON cell (after Yang et al. (1999)). Right: a generic model for stellate cells (after Banks and Sachs (1991)).

The characterization of the active behavior follows the Bank and Sachs (1991) proposal of distribution of HH channels. The parameters of the HH channels are changed so that the spikes match those found experimentally.

The connectivity of the SON model with respect to the CD model is the following: an array of NL cells gives afferent input to an array of SON cells. These in turn project back to the NL cells. The input to the SON from NA is simulated in the same way the input of the NM to the NL is simulated, with the difference that the NA input is not phase locked<sup>9</sup>. The synapses between the NL and the SON produce unitary PSPs (minis) that try to match those in Yang et al. (1999). The synapses between the SON and the NL follow the recommendations of Yang et al. (1999) and Funabiki et al. (1998).

<sup>9</sup> Although a certain degree of phase locking might be expected, specially at very low frequencies (Warchol and Dallos, 1989, 1990).

## The NEURON language simulation approach

NEURON is a simulation environment aimed to model electrical and chemical processes in neurons or networks of neurons (Hines and Carnevale, 1997; website of the project: Carnevale and Hines, 1999). This environment is based on an underlying object-oriented simulation language. This language is defined with functions and variables that are of typical use in neuronal simulation and in the neuroscience field.

The mathematical basis of the simulation involves the solution of cable equations in compartmentalized objects (Rall, 1964). In NEURON compartments are called segments, and they represent finite cables. The segments are grouped into sections (e.g. a dendrite or a soma). The sections can be arranged in order to construct any tree structure that may resemble a neuron. Groups of neurons joined together by synapses create a neural network.

The solution of the differential equations involving the current flow is done in a step-by-step fashion. A numerical method<sup>10</sup> is used with small time steps  $\Delta t$  that may be fixed, or be dynamical for an improved performance.

Channels, synapses and other mechanisms such as current injections or voltage clamps are defined as point processes and they are inserted in sections or segments.

Morphological characteristics are defined at the level of section. General variables, such as the membrane capacitance and the experiment temperature, can be defined globally.

The simulation language is versatile enough so that it allows the definition of customized processes, e.g. special kinds of synapses or modified HH channels. The graphical interface functions allow the construction of a friendly user interface. Hence, the user

---

<sup>10</sup> There is two of choice: backward Euler, and a variant of Crank-Nicholson

could specify different experiments without the need of writing code. For a quick tutorial on NEURON language, see Martin (2000).

### Conceptual implementation of the model by NEURON

At this moment, NEURON presents limitations in spatial design of the neurons. It offers 3-D functions that are ready for drawing geometrically complex sections, but: (1) the 3-D shape is only important when accounting for the total membrane area, and (2) the connectivity can only be disposed in a tree fashion.

The latter fact is of special relevance. The finite cylinders that represent a section are reduced conceptually, for connectivity purposes, to limited lines (segments). The connections between sections can then only be laid out in a restricted way. In our model, the six dendrites are connected to the soma in different 2-D positions. This is not possible in NEURON, since only a 1-D connectivity can be designed.

This restriction makes it difficult to decide a meaningful design for our model. However, the use of a soma that is made of only 1 compartment resolves the conundrum. All connections leading to a compartment lose geometrical distinctions. They all go to the same numerical equation associated to the compartment. A geometrical disposition of connections makes sense when a number of compartments are involved (i.e., in the dendrites), since different equations are solved in every segment.

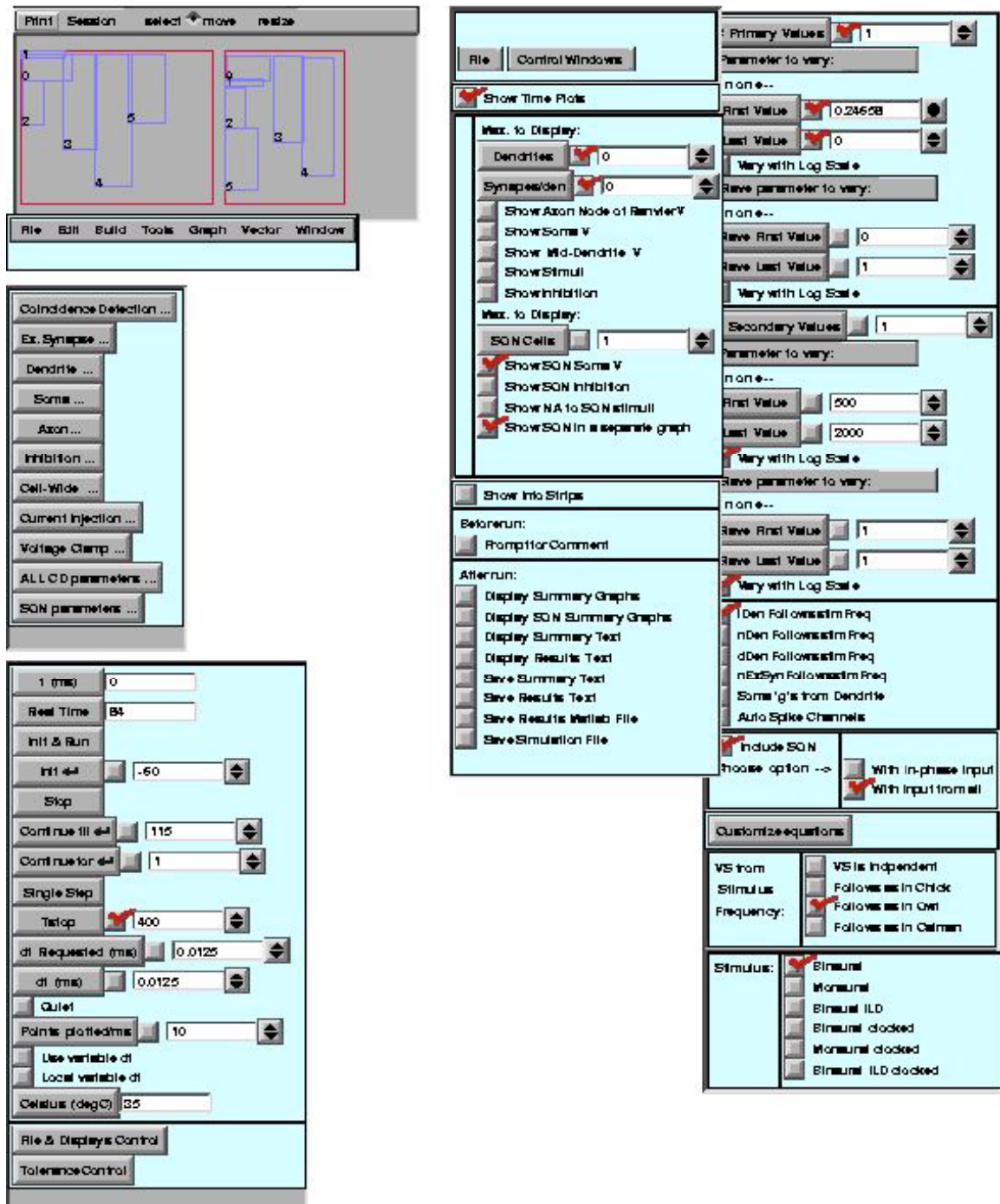


Figure 13. Details of the control panel of the CD+SON simulator.

## Data from Katrina Macleod

In Yang et al. (1999) there is a figure with typical curves of the response of a SON cell to current injections. For the purpose of our analysis, these curves are not clear enough.

Specifically, the behavior of the cell in the first milliseconds is crucial for the characterization of the ball-and-stick model. These details cannot be achieved from this figure; therefore we have used recordings of a typical SON cell by Katrina Macleod<sup>11</sup>.

The recordings comprise six sets with eleven current steps applied per set. The range of currents goes from  $-0.2$  nA to  $0.25$  nA. The sampling rate is 30000 samples/s and the length of the steps is 400 ms. The recordings were made at room temperature,  $22^{\circ}\text{C}$ - $25^{\circ}\text{C}$  ( $72^{\circ}\text{F}$ - $77^{\circ}\text{F}$ ).

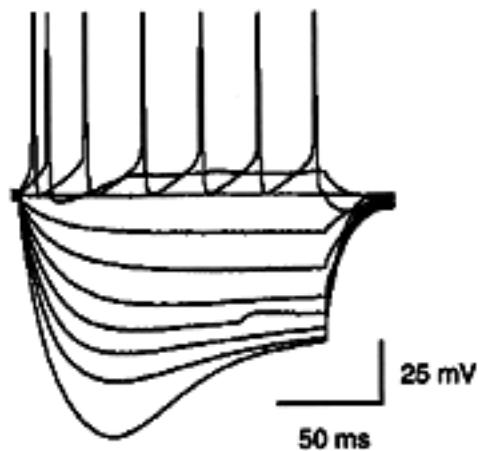


Figure 14. SON cell current injection response curves in Yang et al. (1999).

---

<sup>11</sup> Katrina Macleod is a postdoctoral researcher at the University of Maryland.

CHAPTER III  
Results

## Parameters & actual implementation of the model

The first step in the search for parameters consists in applying the ball-and-stick theory using Macleod's data. This theory says that the response to a current injection in the soma can be approximated by a sum of two exponential functions: the contribution of the soma and the contribution of the dendrites:

$$V_m(t) = C_0 e^{-t/\tau_0} + C_1 e^{-t/\tau_1}$$

The method to derive the values of  $C_0, C_1, \tau_0$  and  $\tau_1$  is explained in chapter 4.5 of Johnston and Wu (1995). Here we are going to give a short outline. Basically, one of the exponentials has a much faster decay than the other. Thus, a logarithmic plot of  $V_m$  becomes a linear function after a certain time because the faster function quickly becomes negligible. The parameters of this linear function lead to  $C_0$  and  $\tau_0$ , since we can write the linear function as:

$$\ln(V_m) = \ln(C_0) - (1/\tau_0)t$$

Where the slope of the function is  $-(1/\tau_0)$  and  $\ln(C_0)$  is the value of the function in  $t=0$ .

Once these parameters are found we can subtract the contribution of their exponential to  $V_m$ .

We can then find the parameters of the other exponential by analyzing the remaining:

$$\ln(V_m) = \ln(C_1) - (1/\tau_1)t$$

We performed this method systematically in all the curves where it was applicable. We left out curves with spikes since we are interested now in passive behavior only.

	Average	St.Dev.
$\tau_0$ (s)	4.14E-02	2.84E-03

$C_0$	3.29E-02	1.48E-02
-------	----------	----------

$\tau$ (s)	1.98E-03	1.42E-04
$C_1$	1.20E+00	3.55E-02

Table 1. Average and st. dev. of the ball-and-stick model parameters in a SON cell.

Using the values from the previous table we can find two parameters of the ball-and-stick model: the electrotonic length of the dendrites ( $L$ ), and the relationship between the impedance of the soma and the output impedance of the dendrite ( $\Delta$ ). The electrotonic length is a parameter that defines the length of a cable with respect to the electric wavelength that is traveling through it. It is thus a dimension-less parameter:

$$L = \frac{l}{\lambda}$$

Where  $l$  is the physical length of the cable and  $\lambda$  is the space constant of the exponential attenuation that the signal suffers with the distance of the cable.

$\Delta$  is called the dendritic to somatic conductance ratio. It is defined as:

$$\Delta = \frac{G_D}{G_S}$$

Where  $G_D$  is the input conductance of the dendrites and  $G_S$  is the conductance of the soma. Since the elements are in parallel, the total conductance of the ball-and-stick model is:

$$G_N = G_D + G_S = G_S(1 + \Delta)$$

In order to compute the value of  $L$  we have to resolve the following equation<sup>12</sup>:

$$\left| \frac{C_1}{(2C_0\tau/l + \tau_0) + C_1} \right| = \cot(\Delta L) [\cot(\Delta L) + 1 / (\Delta L)]$$

---

<sup>12</sup> More on the origin of this equation can be read in Johnston and Wu (1995).

Where:

$$L = \frac{R_N b}{R_i} \sqrt{1 + \frac{R_N}{R_m}}$$

This equation can be solved by simple iterative methods knowing that  $L$  is less than 1 and greater than 0. After solving the equation,  $\lambda$  can be found out with this equation:

$$\lambda = \frac{R_N \cot(L)}{\coth(L)}$$

We applied these equations to the data in the Table 1 and we found the following values:

$L=0.5033$  and  $\lambda=1.667$ .

Once we know these electrical parameters, we are interested in going beyond the ball-and-stick model. We want to specify the morphological characteristics of the cell.

A parameter that is important for that matter is the total area of the cell ( $A_t$ ), which is the area of the membrane that surrounds the cell. We can find  $A_t$  ( $\text{cm}^2$ ) with the following equation:

$$R_m = R_N A_t$$

Where  $R_N$  ( $\Omega$ ) is the input resistance of the cell and  $R_m$  ( $\Omega \cdot \text{cm}^2$ ) is the membrane resistance. The  $R_N$  is the relationship between the current that is injected to the cell and the voltage that the cell acquires in steady state. The membrane resistance,  $R_m$ , is a parameter that relates both the area of the cell  $A_t$  and the input resistance  $R_N$ . It represents the resistance/permeability of the cell membrane per unit area.

$$V_m = I_m R_m$$

Since the membrane of the cell is mainly a lipid bilayer it behaves similarly to an electrical capacitor. The capacity of the whole membrane depends on its area and the capacity density, which is usually  $1 \mu\text{F}/\text{cm}^2$ .

The temporal behavior of the membrane is driven by an exponential function with a time constant  $\tau_m$ (s):

$$\tau_m = R_m C_m$$

Where  $C_m$  is in F/cm<sup>2</sup>.

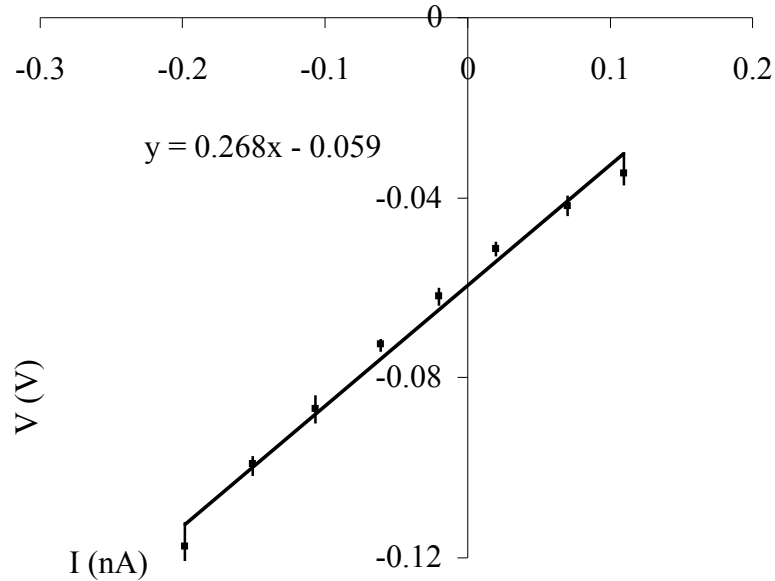


Figure 15. I-V curve of the SON cell in Macleod's data.

$R_N$  and  $\tau_m$  can be computed from Macleod's data analyzing the time constant of the curves and their values in steady state. The  $R_N$  is simply the slope of the line that relates the current injected and the voltage in steady state:

$$V_m = 0.268I_m - 0.059$$

Where  $V_m$  is in V and  $I_m$  is in nA. The  $R_N$  is the slope,  $R_N=268M\Omega$ , and the value of the line when  $I=0$  is called the resting potential,  $V_m(I_m=0) = -59mV$ .

$\tau_n$  can be quantified redefining the current injection curves as being a single exponential decay (while we considered it a sum of two curves for the sake of the ball-and-stick model):

$$V_m(t) = V_m e^{-t/\tau_n}$$

Measuring the decay of the curve in 2 points and computing the average for all the curves we find the value of  $\tau_n$ :  $\tau_n = 33.23 \pm 3.46$  (ms). Hence:

$$R_m = \tau_n / C_m = 33230 \text{ } \Omega \text{ cm}^2$$

And we can find then the  $A_t$ :

$$A_t = R_m / R_N = 12300 \text{ } \Omega \text{ m}^2$$

Now is when we have to rely on the morphological characteristics of our model to derive the rest of its dimensions. To help with this we recall that the factor  $\lambda$  relates the input impedance of the dendrites and the input impedance of the soma. We also know the value of  $L$ , which limits the size of the dendrites for a given  $\lambda_{den}$ . Where  $\lambda_{den}$  is defined as:

$$\lambda_{den} = \sqrt{\frac{d_{den} R_m}{4 R_i}}$$

Where  $d_{den}$  (cm) is the diameter of the dendrite, and  $R_i$  is the intracellular resistance ( $\Omega \cdot \text{cm}$ ). The  $R_i$  represents the difficulty for the ions to circulate across the cell. We fix the value of  $R_i$  to  $200 \text{ } \Omega \cdot \text{cm}$ , which is a reasonable value and it is consistent with the  $R_i$  in the CD model.

The electrotonic length of a dendrite is:

$$L_{den} = \frac{l_{den}}{\lambda_{den}}$$

The total electrotonic length of the dendrites is the sum of the 6 individual electrotonic lengths, which we have assumed are equal.

$$L_{eq} = \sum_{i=1}^6 L_{den}$$

Hence, the electrotonic length of the dendrites,  $L_{eq}$ , depends on two variables: the dendritic diameter and the dendritic length. To constrain the problem more, we add a new equation that helps computing the conductance of a cylinder, in our case the cylinder that represents the dendrites:

$$G_{eq} = (\pi / 2)(R_m R_i)^{1/2} (d_{eq})^{3/2} \tanh(L_{eq})$$

In order to find the  $G_{eq}$  we need to find first the  $d_{eq}$ , following the method of dendritic integration by Rall (Rall, 1959):

$$(d_{eq})^{3/2} = \sum_{i=1}^6 (d_{den})^{3/2}$$

Again, we have that the  $G_{eq}$  depends both on the  $d_{den}$  and the  $l_{den}$  (by means of the  $L_{eq}$ ).

$G_{eq}$  is a value that we know thanks to the  $\pi$  and the ball-and-stick model structure:

$$G_N = G_{Soma} + G_{eq}$$

$$G_N = \frac{G_{eq}}{\pi} + G_{eq}$$

$$G_{eq} = G_N / \left( \frac{1}{\pi} + 1 \right)$$

Where  $G_N$  is simply  $1/R_N$ .

The overall picture shows us that we have two functions of two variables ( $l_{eq}$  and  $d_{eq}$ ), which may have only one solution. However, there is an additional requirement since the

$d_{eq}$  and  $l_{eq}$  are constrained with a fixed total membrane area,  $A_t$ . A trade off might be inevitable.

The somatic area can be extracted from previous studies on the size of the SON cell soma. Carr et al. (1989) reported two types of cells with the following sizes:  $350 \mu\text{m}^2 \pm 62 \mu\text{m}^2$  (number of cells measured,  $n=25$ ) and  $209 \mu\text{m}^2 \pm 33 \mu\text{m}^2$  ( $n=27$ ). Lachica et al. (1994) reported that the SON cells are of average size  $254 \mu\text{m}^2 \pm 57 \mu\text{m}^2$ .

Therefore, an average value of  $265 \mu\text{m}^2$  seems reasonable. This value, due to the technique used to measure the soma (camera lucida), is a horizontal section of the soma. If we approximate the soma as a sphere, then the somatic area corresponds to the area of a cross-section of the sphere: a circle<sup>13</sup>. Hence, the diameter of the soma is approximately  $d_{soma}=18 \mu\text{m}$ .

The equations that remain to be solved are:

$$\begin{aligned} G_N / (1/\lambda + 1) &= (\lambda/2)(R_m R_i)^{\lambda/2} \left( \int (d_{den})^{3/2} \right) \tanh(L_{eq}) \\ L_{eq} &= \int (l_{den} / \sqrt{(d_{den} R_m) / (4R_i)}) \\ R_m &= A_t R_N = (A_{soma} + A_{axon} + A_{den}) R_N = (A_{soma} + A_{axon} + \lambda d_{den} l_{den}) R_N \end{aligned}$$

After a process of twitching  $d_{den}$  and  $l_{den}$  the best fit we have found is this:  $d_{den}=4.8 \mu\text{m}$  and  $l_{den}=120 \mu\text{m}$ . The error that this trade-off yields in  $R_m$  and  $L$  is very low and inside standard deviation margin. The error associated to  $R_m$  is a 0.6% and the error associated to  $L$  is a 1.3%. It is interesting to point out that the straight application of the 3 equations yields an uninteresting result ( $d_{den}=5 \mu\text{m}$ ,  $l_{den}=983 \mu\text{m}$ , average number of dendrites=0.737) given what we know about the morphology of the SON cell. Thus it

<sup>13</sup> In fact, NEURON constructs spheres as cylinders of diameter and height equal to the diameter of the sphere. Thus, the membrane area of the cylinder and the sphere are the same, since the top and the bottom seals of the cylinder are disregarded.

seems better for us to establish a fixed number of dendrites and accept an approximate fitting.

Once we have found out the morphological parameters of the soma and the dendrite we still need the parameters related to the axon. In this case, and due to lack of information, we are going to follow the guidelines of the Banks and Sachs (1991) model. In that model the axon is small (is important to remember that ‘small’ is referred to its electric properties, not to its physical size) and has little influence in the global impedance of the cell. Moreover, when we were applying the ball-and-stick approach we were disregarding the axon influence in the soma. Consequently, we have to assign a small size to the axon. In our case we have chosen  $l_{axon}=40 \mu\text{m}$  and  $d_{axon}=d_{den}=4.8 \mu\text{m}$ , which are values that are in the threshold of influence.

Now the cell is completely defined in its morphological aspects. The next step is to define its active characteristics: the parameters of the HH model.

The parameters of the HH model that we can resolve mathematically are those which influence the passive behavior of the cell:  $g_{lsoma}$ ,  $g_{lden}$  and  $g_{laxon}$ . They are the inverse of the impedance of their sections:

$$g_{lden} = G_{eq} = 1.637E-05$$

$$g_{lsoma} = (\pi / 2)(R_m R_i)^{\pi/2} (d_{soma})^{3/2} \tanh(L_{soma}) = 6.286E-04$$

$g_{lsoma}$  is computed as the conductance of a cylinder, since NEURON creates it as such.

$g_{laxon}$ , as we said before, is disregarded in the ball-and-stick model and thus we are going to give it a conservative value of  $g_{laxon}=g_{lden}$ .

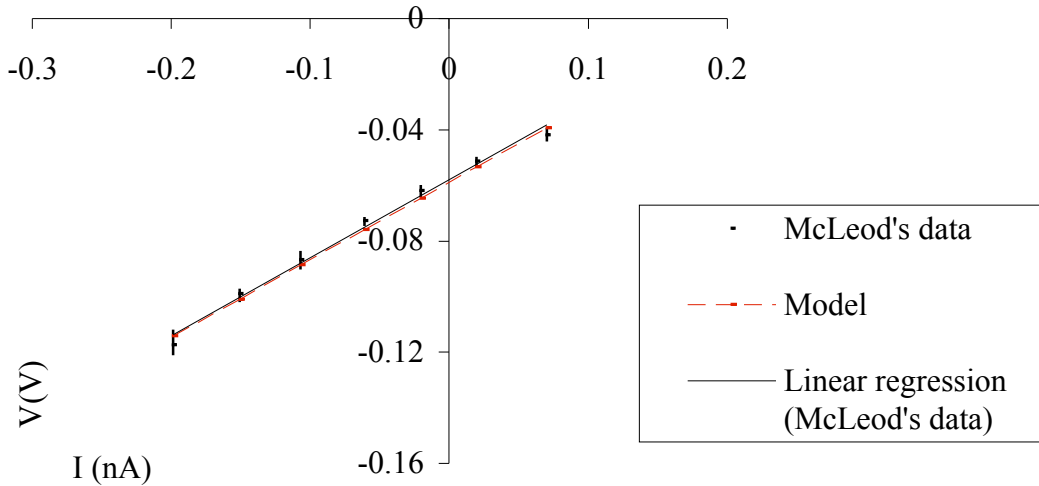


Figure 16. Comparison of the model response to a current injection and averaged empirical recordings from Macleod's data.

As can be seen in the chart, the error of the model is low if we compare it to the linear regression adjusted to Macleod's data. Nevertheless, the model presents an average error of  $0.96 \text{ mV} \pm 2.59 \text{ mV}$  with respect to Macleod's data. Non-linearities in the empirical data lead to the error of  $\pm 2.59 \text{ mV}$  in the standard deviation. Intrinsic properties of the model lead to an average error of  $0.96 \text{ mV}$ . The latter may have multiple reasons, e.g. the influence of the axon or too general assumptions in the ball-and-stick model. But it is also important to remember that the parameters of the ball-and-stick model already were a trade-off and carried an associated error of 1.3%. Therefore, the average error is mainly due to our initial trade-off.

The rest of the HH parameters have to be found in the simulator and they are explained in the next section. It is important to observe that the error associated to the passive scheme increases with the current, being of between 2-3 mV with higher currents. That's going to be a vital factor in the next section.

## Parameters found empirically

From the curves of Macleod's data we choose the one that is closer to the average parameters. That is the  $s3$  set of curves<sup>14</sup>:

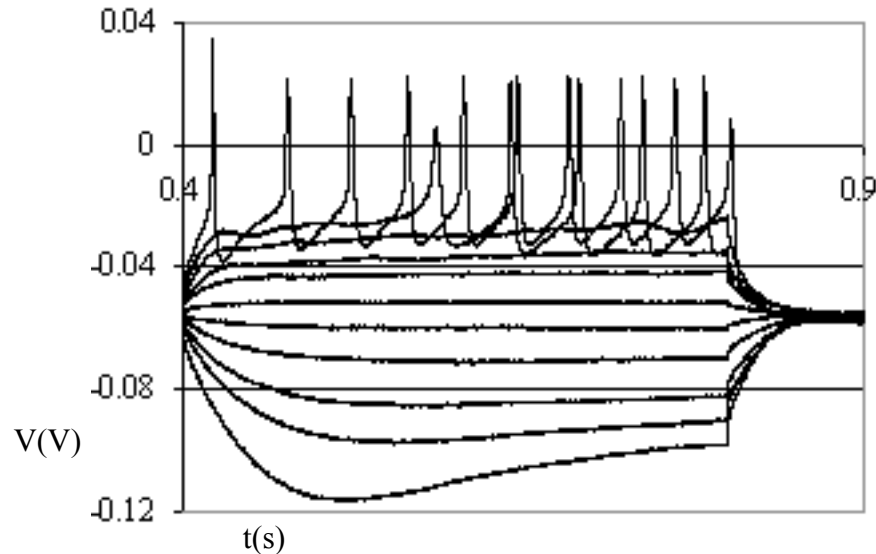


Figure 17. Set of curves  $s3$ .

In our model, we are primarily interested in adjusting the HH parameters so that its spike rate is similar to that of the  $s3$  curves. To start with, we choose to set as initial values of the HH model those found in the experiments of Hodgkin et al. (1952) (see also Johnston and Wu, 1995)<sup>15</sup> in the squid giant axon. Then we will go step by step particularizing the parameters for our case:

(Step 1) Decreasing spiking rate.

The HH model presents a high spiking rate compared to that of the SON cells. To decrease the spiking rate, the best way is to slow down evenly the time parameters of the

---

<sup>14</sup> The 11 set of curves are labeled  $s0, s1, s2\dots$

<sup>15</sup> With  $g_{Na}=2 \text{ S/cm}^2$  and  $g_K=0.5 \text{ S/cm}^2$ , both in the soma and the axon.

HH model. In our case, the curve with higher current injection is the reference. This curve has a spiking rate of approximately 25 spikes/s. The parameters with timing information are those with a 0 in the name (i.e.  $\tau_0$ ,  $\tau_{h0}$ , etc.). We attained the desired spike rate roughly dividing them by 40.

(Step 2) Increase threshold of spike triggering.

The spikes of the SON model are triggered at voltages quite higher than in the HH model. To change this situation we increase all the parameters that contain information about the median voltage at which a channel is open. This effectively raises the voltage at which a channel is triggered. These parameters are distinguished in the model by having a ‘VHalf’ particle in the name (i.e.  $\tau_{VHalf}$ ,  $\tau_{mVHalf}$ , etc.). The threshold to trigger the first spike in  $s3$  is of about  $-23$  mV. This threshold can be met with a raising 45mV the median voltages<sup>16</sup>. The  $g_{Na}$  now needs to be raised temporally to trigger spikes.

(Step 3) Reduce spike width.

After setting a higher  $g_{Na}$ , the spikes are of a larger than desired width. Spikes in  $s3$  are of about 3 ms wide at 0 mV. A way of decreasing this is to lower the  $g_{Na}$  while increasing  $\tau_{0K}$ . The rationale of this is that  $g_{Na}$  controls the overall rising of the spikes. Decreasing it makes it difficult for the current to reach threshold. However, a  $\tau_{0K}$  increase makes the cell charge faster at lower levels and counteracts the  $g_{Na}$  decrease. Furthermore, a decrease in  $\tau_{0K}$  allows the spiking decay to be faster.

---

<sup>16</sup> With a  $g_{Na}$  fairly stronger, i.e.  $g_{Na}=8$  S/cm<sup>2</sup>.

We multiply  $\tau_{0K}$  by 8,  $\tau_{0K}=0.025 \text{ ms}^{-1}$ , and  $g_{Na}$  goes from  $8 \text{ S/cm}^2$  to  $0.3 \text{ S/cm}^2$ . The spikes are now of about 7 ms wide at 0 mV. These two parameters also regulate the voltage at the lowest point between spikes, which in Macleod's data is of about  $-33 \text{ mV}$ .

(4) Reduce further the spike width.

Other parameters that can be manipulated to change the spike width are  $\tau_{0K}$  and  $\tau_{h0Na}$ . An increase in  $\tau_{0K}$  leads to a quicker spike rise and, specially, a quicker decay. An increase of  $\tau_{h0Na}$  leads to smaller and shorter spikes. With these parameters we have to be careful controlling the spike height, which is of an average of 21 mV.

Steps (3) and (4) have to be performed repeatedly, in a process of approximation.

Moreover, the pair  $g_{Na}-g_k$  has to be tuned, and changing one of them influences the effect of the other.

Not only do all the constraints above need to be met (or approximated), but we also need to make sure that the curves representing injections of low currents do not spike. The error coming from the ball-and-stick model makes the task even more difficult. The best results we have attained are:

	Attained	Macleod's data
Spike threshold	-23 mV	-23 mV
Period between spikes	38 ms	40 ms
Spike width	4 ms	3 ms
Minimum between spikes	-36 mV	-33 mV
Spike height	18 mV	21 mV

Table 2. Degree of approximation of the model to the empirical recordings.

It is convenient to realize the limitations of the model in the characterization of the  $\text{Na}^-$  and  $\text{K}^+$  channels. A quick glance at Macleod's data shows us a clear example of this.

There is a very long latency time in the second-to-last curve (the second with most current) of the set  $s3$ . Such a latency time of flagging oscillation can hardly be expected from the HH model.

One of the most challenging parts in the quest of finding the best parameters is the fact that the spike width is comparatively very small with respect to the signal period. The rising of a spike has to be initially long, while avoiding the apparition of spikes in non-spiking curves. At the same time, the raising has to be fast enough in the peak so that the width of the spike is small enough at 0 V.

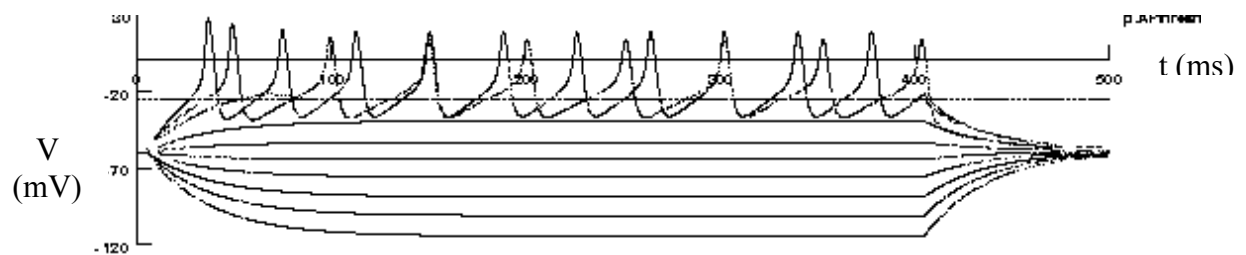


Figure 18. Set of curves of the SON model.

After the active parameters are decided, the SON cell is completely defined (see Appendix B). The next parameters needed are those related to the synaptic connections with other cells.

### Synaptic connections

To relate our SON cell to the rest of the model we are interested in finding the characteristics of the synapses. The smallest PSP (a “mini”) that can be generated in a synapses helps us to model mathematically.

In Yang et al. (1999) there's a study of the PSPs that the NL creates in the SON. In particular we are interested in the smallest that can be generated (p. 2317, fig. B, trace in the bottom right). That PSP has a height of 3.3 mV and a length of 15 ms.

The equation modeling a synaptic input that we are going to use is defined by:

$$i = g(v - E_r)$$

$$g = k \frac{t}{\tau} e^{-\frac{t}{\tau}}$$

Where  $g$  (S) is the conductance change in the cell caused by the synaptic input,  $E_r$  (mV) is the reversal potential of the synapse, and  $g_{\max}$  (S) and  $\tau$  (s) are parameters that control the size of the synaptic input and which are selected by means of simulation.  $g_{\max}$  is maximum conductance change that the synapse elicits and  $\tau$  is the time constant of the synapse.

The simulation consists in creating a spike in the NL cell (e.g. with a current injection) and observing the voltage in the SON cell. After this is done we choose as parameters  $g_{\max}=0.009$  S and  $\tau=0.45$  ms.

The reversal potential  $E_r$  is not given in the literature, a reasonable value for an excitatory synapse would be  $E_r=-10$  mV. A synaptic input will be triggered when the voltage at the NL cell axon tip surpasses the  $-25$  mV threshold, which is the threshold to count a spike in the NL cell. The latency time for a PSP to appear is reported in Yang et al. (1999) as 2.6 ms.

It is interesting to point out that these PSPs can be regarded either as coming from the NL or from the NA. The electrical stimulus was located in the fiber tract that includes both NL and NA fibers.

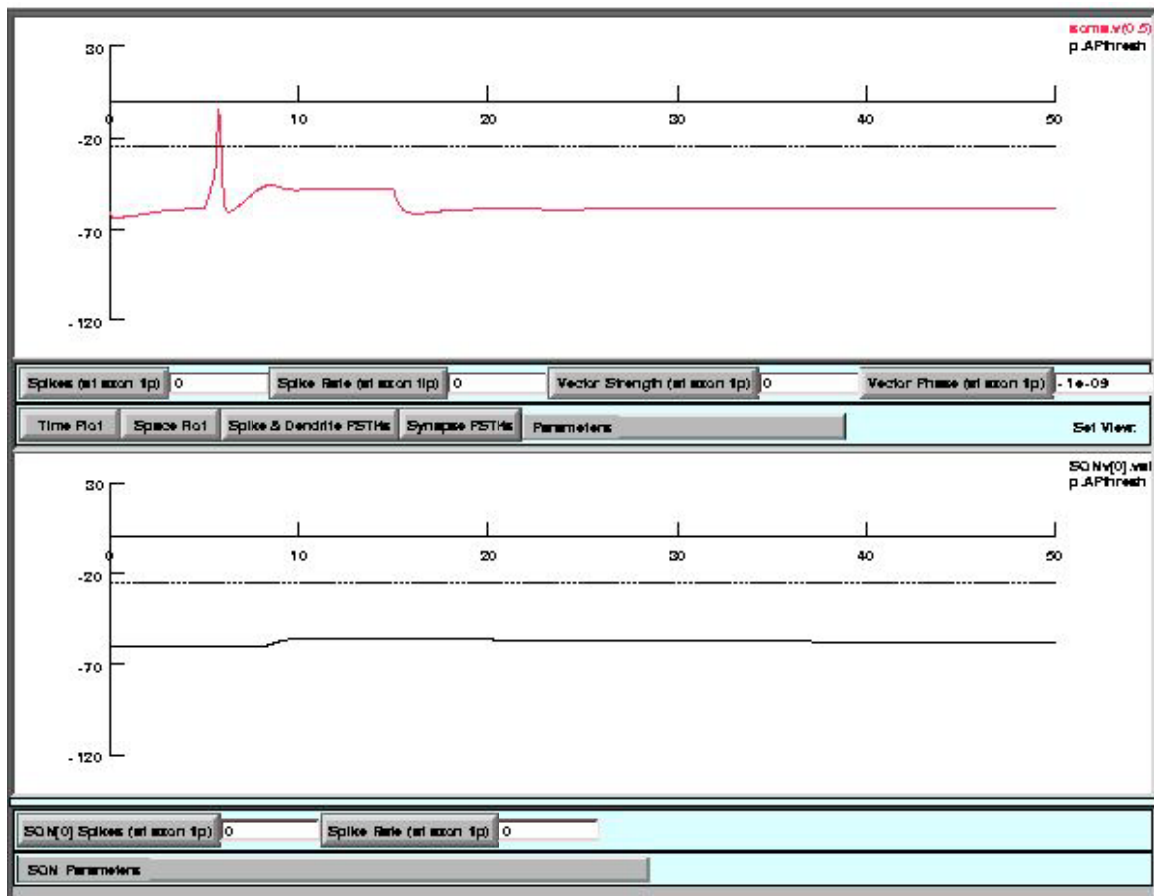


Figure 19. Simulation of a postsynaptic response in a SON cell after excitation with a current injection of 0.7 nA and 10 ms. The NL cell has a best frequency of 2000 Hz.

The connection from the SON to the NL is a bit more complex to characterize. Both Funabiki et al. (1998) and Yang et al. (1999) described the characteristics of these synapses, which are of GABAergic nature. Funabiki et al. (1998) stated that the conductance change due to synaptic input was very variable and that it was of  $4.3 \text{ nS} \pm 3.0 \text{ nS}$ , in a survey of cells with an average conductance of  $3 \text{ nS}$  ( $\Delta g = g_{\text{max}} = 3 \text{ nS}$ ). This means a median decrease of a 59% in the impedance. This change of conductance is considerable large and the NL cell improves greatly its resolution. They also described

the synaptic input as having a fast rise time constant ( $\tau_r=15 \text{ ms} \pm 7 \text{ ms}$ ) and a slow decay time constant ( $\tau_d=106 \text{ ms} \pm 44 \text{ ms}$ ). This can also be noticed in Yang et al. (1999).

The reversal potential is hypothesized to be depolarizing *in vivo* in Funabiki et al. (1998).

A depolarizing reversal potential leads to an inhibition that is unaccustomed. Usually, inhibition is regarded as an input that lowers the conductance of a cell, hindering the apparition of new spikes and inactivating sodium channels. Yang et al. (1999) gave a magnitude for the reversal potential,  $E_r=-34 \text{ mV}$ . When the cell voltage is under that value, the input from the SON is of a depolarizing nature, and conversely. This helps the cell not only to increase the conductance but also to inactivate the sodium channels (Monsivais and Rubel, 2001).

To implement this synaptic input in our model we use a class of synapses with 2 time constants:

$$i = g(v - E_r)$$

$$g = k \left[ e^{-\frac{t}{\tau_2}} - e^{-\frac{t}{\tau_1}} \right]$$

The experiment to find its parameters is a short current injection in the SON cell that triggers a spike. Our NL cells have an input impedance  $R_N=72 \text{ M}\Omega$  ( $g_N=9.4 \text{ nS}$ ) (based on Reyes et al. (1996)), which is far lower than that measured in Funabiki et al. (1998). A 59% decrease of impedance in our NL cell would lead to a conductance of  $3.4 \text{ nS}$  ( $\tau_g=g_{\max}=6 \text{ ns}$ ). On the other hand, Yang et al. (1999) show a trace that could be that of a mini (p. 2319, fig. A, top), but it is not clear.

Nonetheless, the simulation seems to be somehow consistent with the conductance change measured by Funabiki et al. (1998) and by Yang et al. (1999). However, the two

studies seem to disagree partially in the timing. We are convinced that the large difference between the  $R_N$  of Funabiki et al. (1998) and Reyes et al. (1996) comes from the limitation of Reyes et al. (1996) study, which is bounded to high frequency cells (800-3000 Hz). We are going to use Yang et al. (1999) timing data because they seem to be consistent with high frequency NL cells. Funabiki et al. (1998) data seem to be more consistent with a general survey of NL cells.

The rise time in Yang et al. (1999) is of about 7 ms, and the 50% decay time is of about 73 ms. We choose  $\tau_r=4$  ms and  $\tau_d=60$  ms,  $g_{max}=6$  nS. Yang et al. (1999) also reported a long latency time for the apparition of a PSP (7-12 ms). Therefore we choose a latency of 9.5 ms.

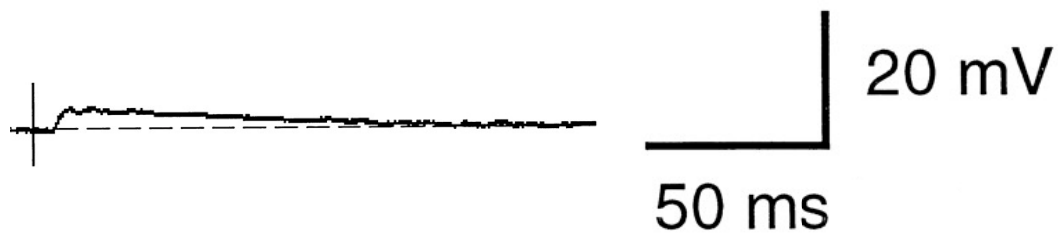


Figure 20. Typical intracellular PSP recording of a NL cell while electrically exciting SON cells (after Yang et al. (1999)).

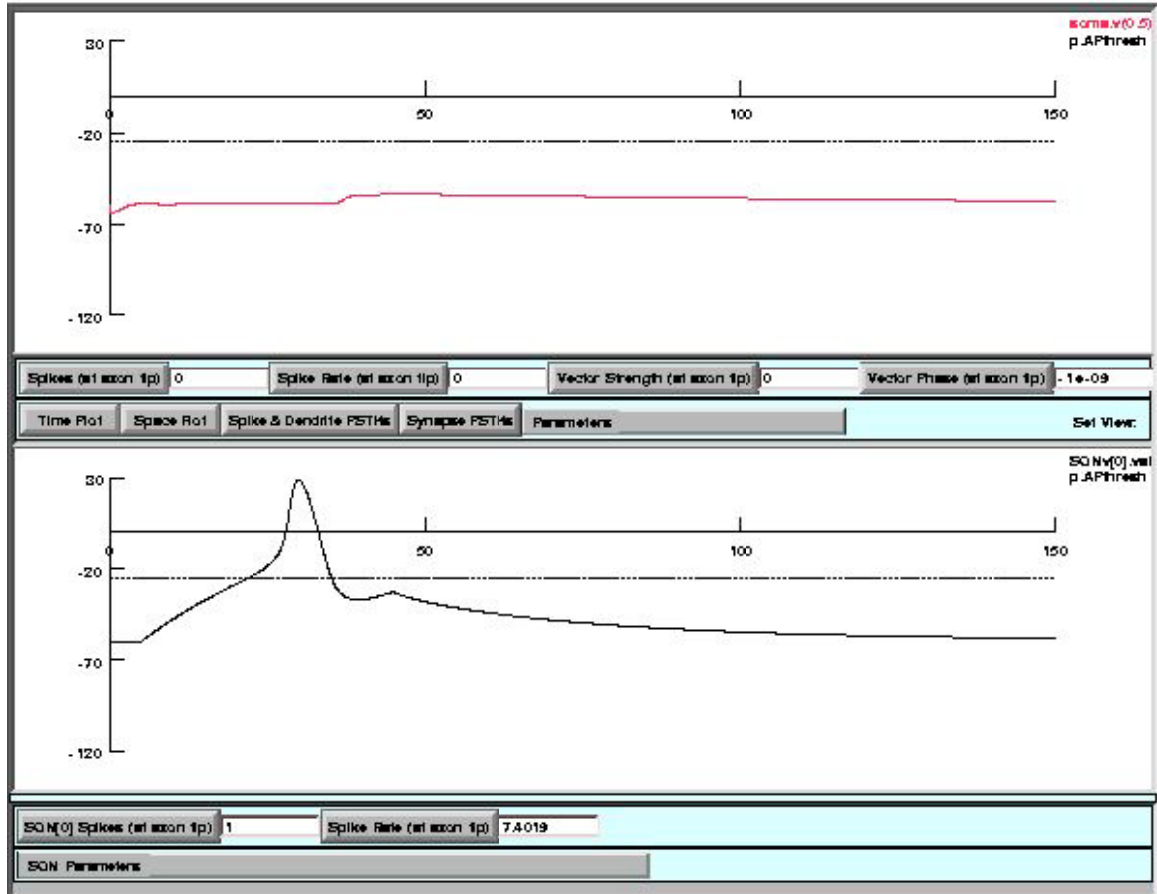


Figure 21. Simulation of a postsynaptic response in NL after injecting a current of 0.3 nA and 40 ms in a SON cell.

The number of connections between the SON cells and the NL cells is not known. In Yang et al. (1999) a summation of PSPs (postsynaptic potentials) seems to occur. Thus we can argue that there might be a number of synapses involved. However, nothing conclusive can be drawn from this data. For our simulation purposes we have chosen to have one synapse per SON dendrite in principle.

The last part of the model that needs tuning is the NA input to the SON. This input, as we said above, resembles that of the NM to the NL. The difference is that the NA input is not

phase-locked. In general, its characteristics will be approximated experimentally when assessing the performance of the model.

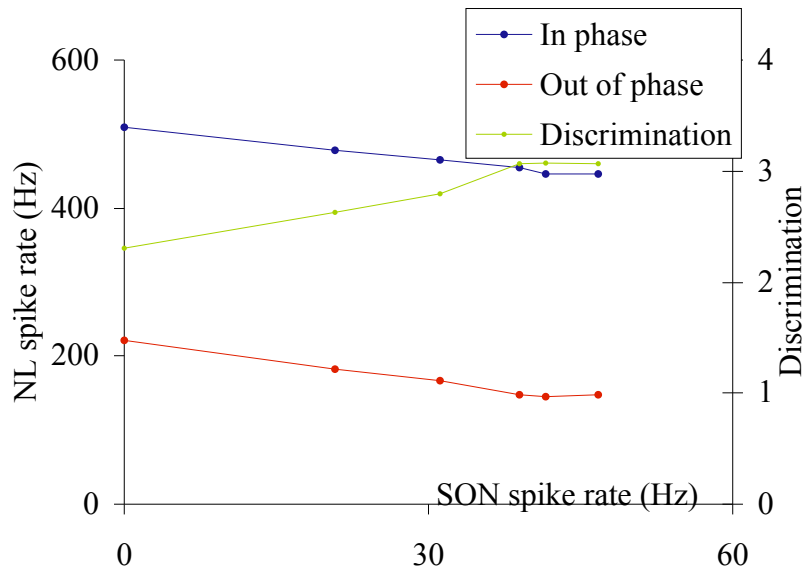
### The CD+SON model performance

A first test for the CD+SON model is going to be exciting the SON cell with a current injection and observing what is the effect in the NL cell. Thus, we connect the output of 1 SON cell to 2 NL cells (one in-phase and the other out-of-phase). We excite the SON cell with a current injection of different amplitudes, and the NL cell with a sound of different frequencies.

In the next chart we can appreciate the effects of the SON cell output in the NL cells. The sound source has a frequency of 700 Hz and the NM input involves well-timed spikes ( $\tau=0.1111$ ).

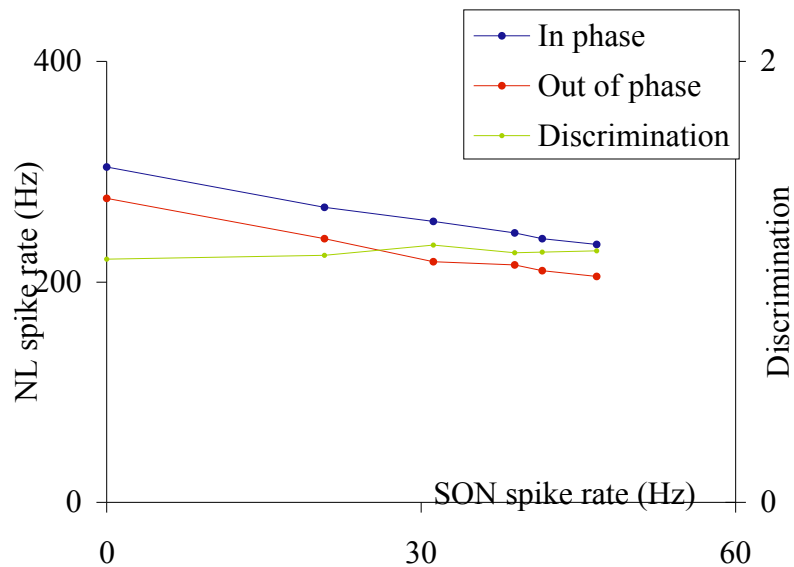
Specific parameters of the simulation:

Frequency=700 Hz	$g_{\max}=0.08 \mu\text{S}$	$\tau=0.1111 \text{ ms}$	VS as in chicken
------------------	-----------------------------	--------------------------	------------------



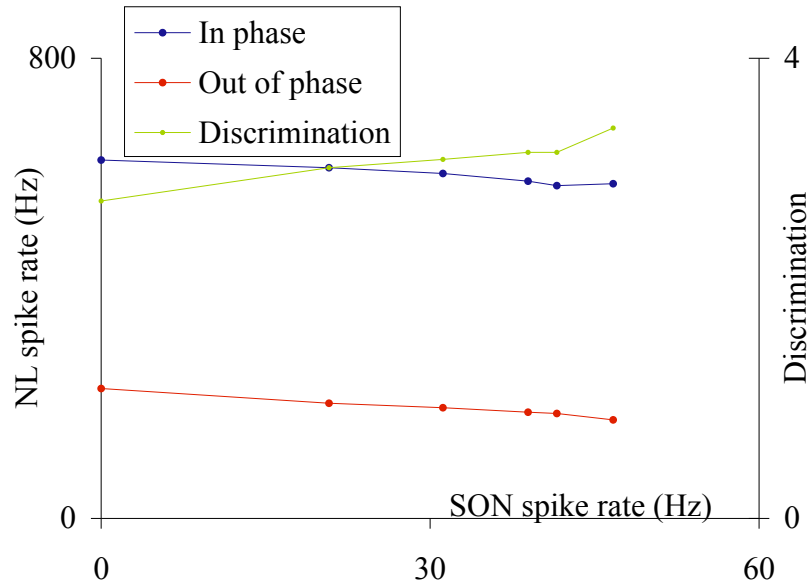
Effect of SON cell spiking in a NL cell with a 700 Hz sound. The rightmost sample corresponds to a current injection in the SON cell of 0.6 nA.

Frequency=2000Hz	$g_{max}=0.08 \mu S$	$\tau=0.1111 \text{ ms}$	VS as in chicken
------------------	----------------------	--------------------------	------------------



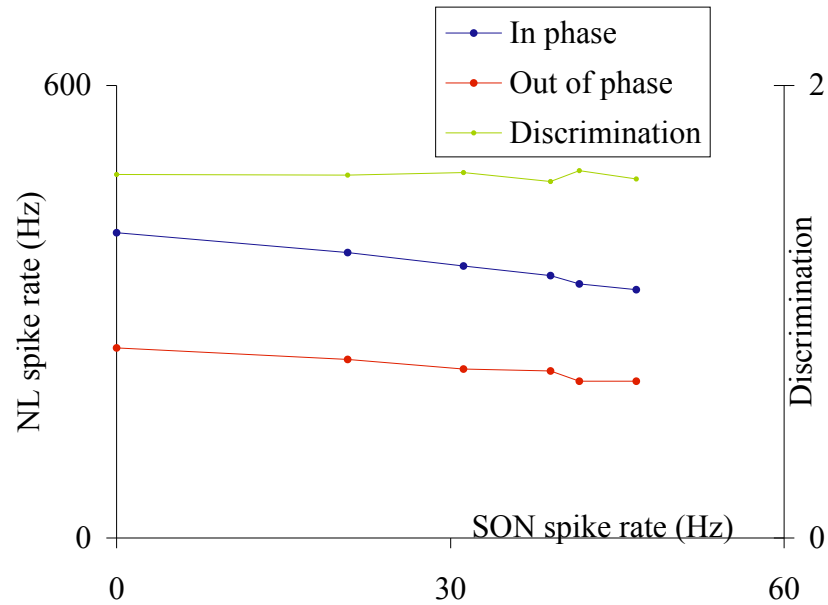
Effect of SON cell spiking in a NL cell with a 2000 Hz sound. The rightmost sample corresponds to a current injection in the SON cell of 0.6 nA.

Frequency=700 Hz	$g_{\max}=0.08 \mu\text{S}$	$\tau=0.1111 \text{ ms}$	VS as in owl
------------------	-----------------------------	--------------------------	--------------



Effect of SON cell spiking in a NL cell with a 700 Hz sound. The rightmost sample corresponds to a current injection in the SON cell of 0.6 nA.

Frequency=2000Hz	$g_{\max}=0.08 \mu\text{S}$	$\tau=0.1111 \text{ ms}$	VS as in owl
------------------	-----------------------------	--------------------------	--------------

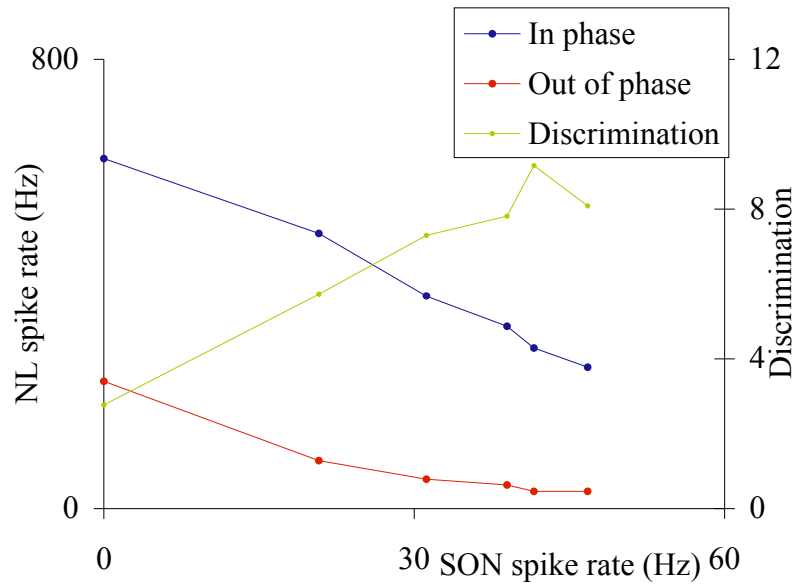


Effect of SON cell spiking in a NL cell with a 2000 Hz sound. The rightmost sample corresponds to a current injection in the SON cell of 0.6 nA.

The discrimination is the ratio between the spikes in the in-phase cell and the out-of-phase cell. As we can observe from the previous charts the SON reduces the number of spikes in both in-phase and out-of-phase cells by a similar magnitude. An improvement in the discrimination can thus appear. While the reduction is of similar magnitude to both, the ratio becomes more favorable to the in-phase.

The next experiment is a repetition of the previous, with the difference that we increase the number of SON cells to 5.

Frequency=700 Hz	$g_{\max}=0.08 \text{ } \mu\text{S}$	$\tau=0.1111 \text{ ms}$	VS as in owl
------------------	--------------------------------------	--------------------------	--------------



Effect of SON cell spiking in a NL cell with a 700 Hz sound. The rightmost sample corresponds to a current injection in the 5 SON cells of 0.6 nA.

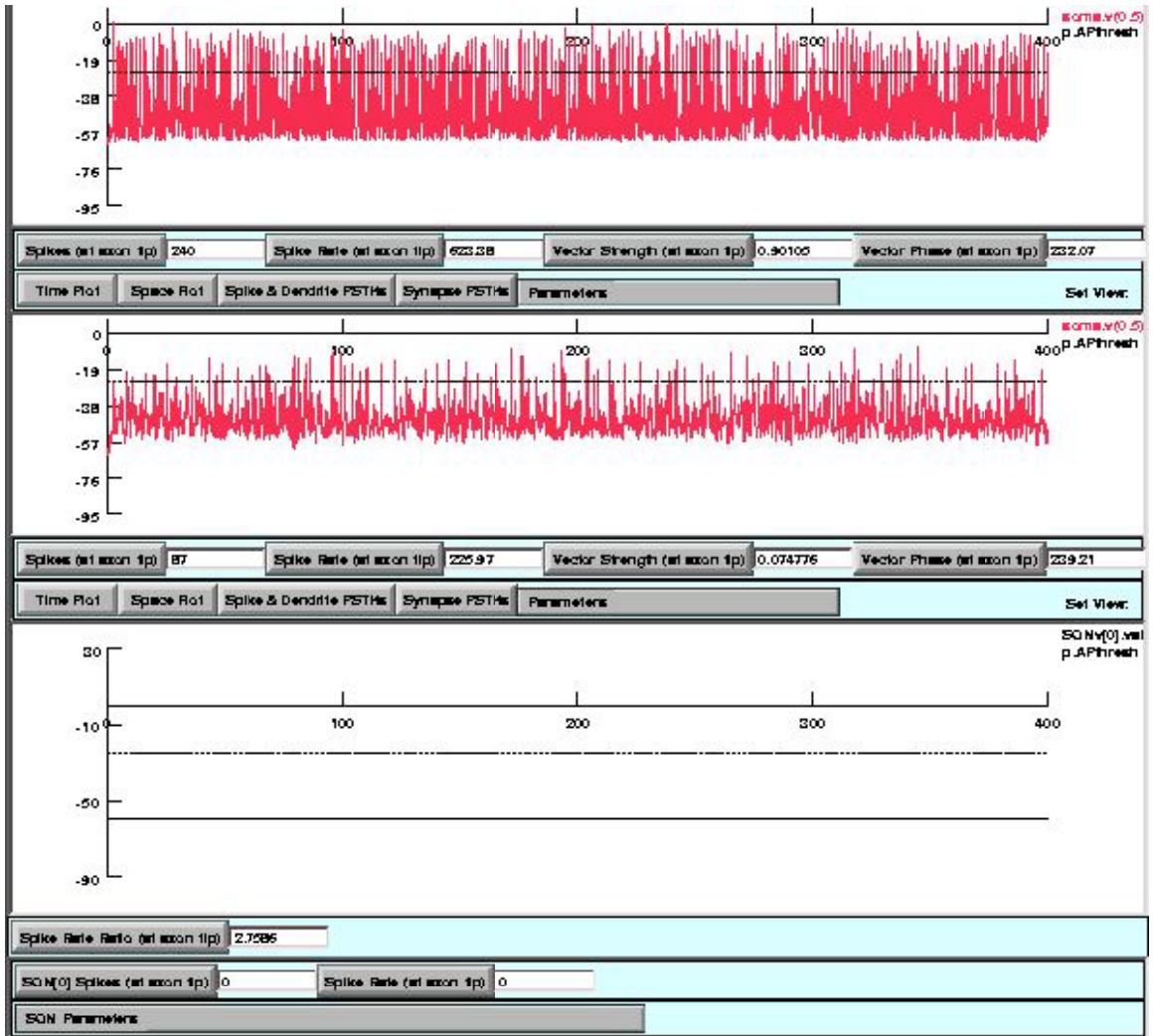


Figure 22. NL cell excited with inputs phase locked to a tone of 700 Hz and without SON inhibition.

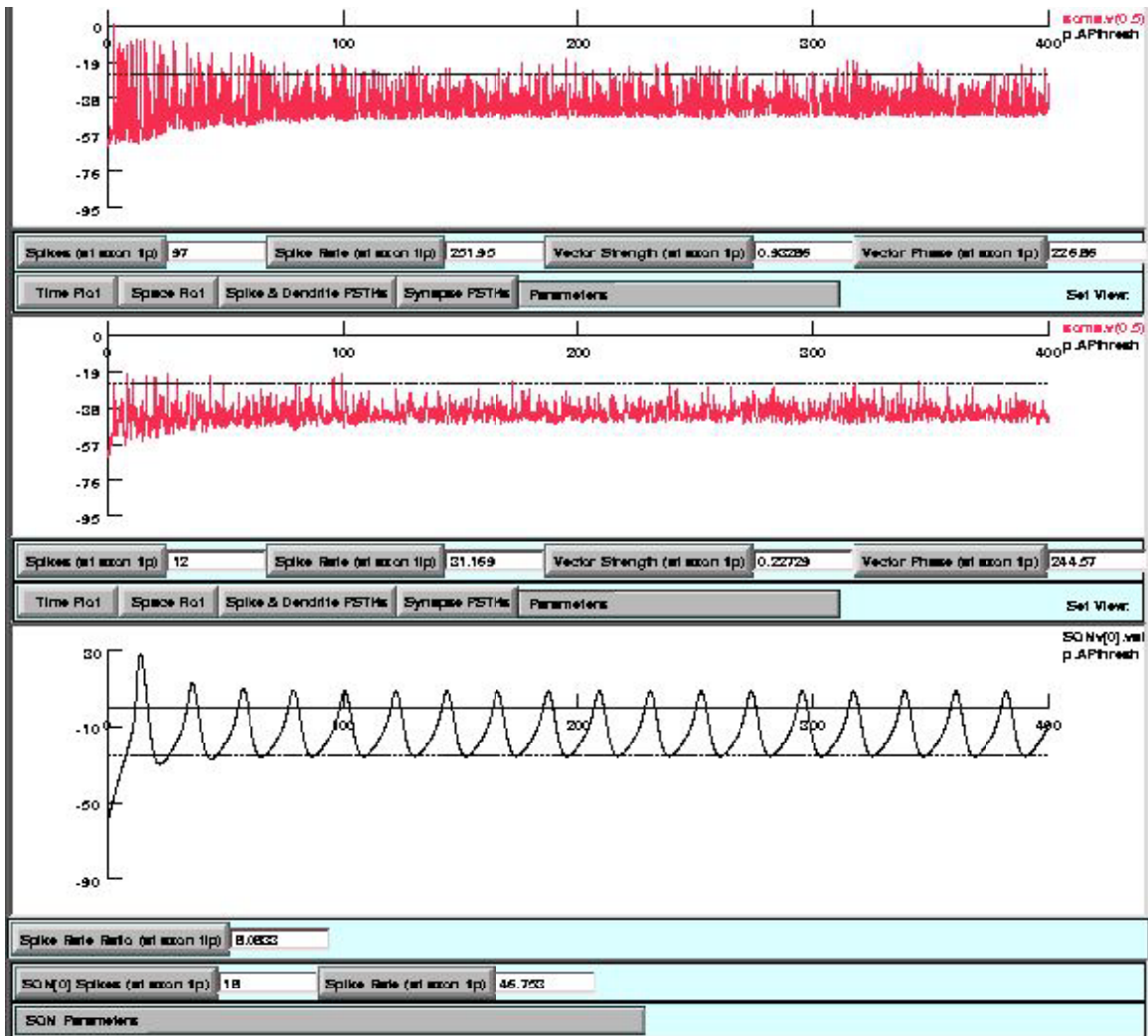
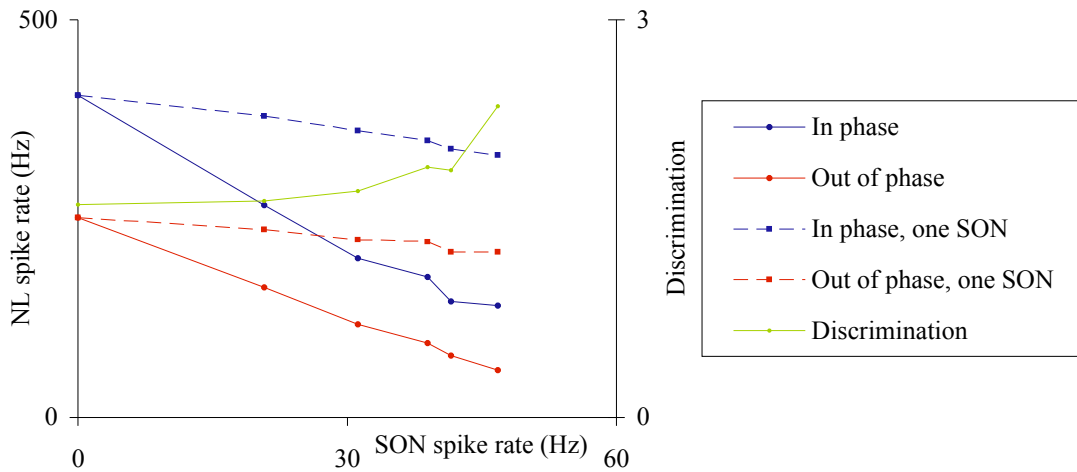


Figure 23. NL cell excited with inputs phase-locked to a sound of 700 Hz and receiving the inhibition of 5 SON cells that are excited with a current injection of 0.6 nA.

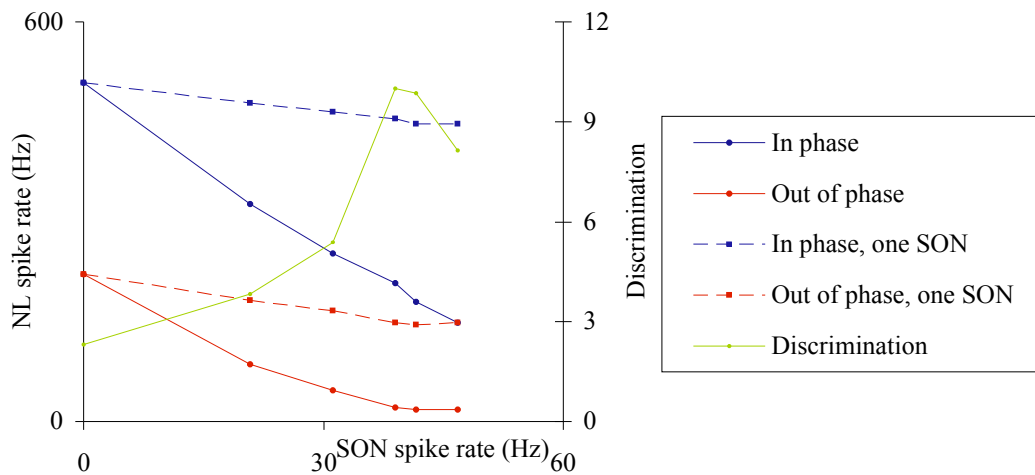
Frequency=2000Hz	$g_{\max}=0.08 \mu\text{S}$	$\tau=0.1111 \text{ ms}$	VS as in owl
------------------	-----------------------------	--------------------------	--------------



Effect of 5 SON cell spiking in a NL cell with a 2000 Hz sound.

Comparison to the 1 SON cell case.

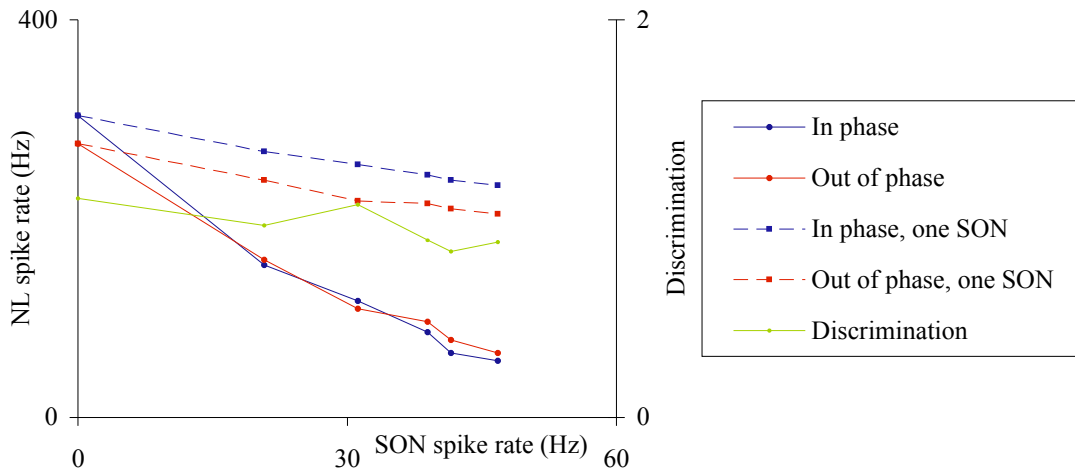
Frequency=700 Hz	$g_{\max}=0.08 \mu\text{S}$	$\tau=0.1111 \text{ ms}$	VS as in chicken
------------------	-----------------------------	--------------------------	------------------



Effect of 5 SON cell spiking in a NL cell with a 700 Hz sound.

Comparison to the 1 SON cell case.

Frequency=2000Hz	$g_{\max}=0.08 \mu\text{S}$	$\tau=0.1111 \text{ ms}$	VS as in chicken
------------------	-----------------------------	--------------------------	------------------



Effect of 5 SON cell spiking in a NL cell with a 2000 Hz sound.

Comparison to the 1 SON cell case.

As can be appreciated from these experiments a stronger SON input leads to a better discrimination in most cases, except when the discrimination is too low ( $\leq 1$ ) to begin with. In those cases, the effect of the inhibition does not improve the ratio. These results coincide broadly with the experiments of Bruckner and Hyson (1998) in NL neurons of the chicken. In those experiments they manipulated the concentration of GABA and noticed the changes in coincidence detection: “GABA had contrary effects on the S-ITD [simulated ITD] functions depending on the drug concentration. A low GABA dose enhanced excitability at favourable S-ITD, but not at unfavourable S-ITDs. In contrast, higher GABA concentrations diminished excitability. Moderate GABA concentrations had no consistent effect.” As we have seen we can add nuances to this assertions.

One suggestion from Bruckner and Hyson (1998) that could not be appreciated in the above simulations is that some NL cells increase excitability with low GABA concentrations.

It is interesting to notice that the best improvement when we increase the number of SON cell inputs to NL occurs with both high frequency (2000 Hz) and good phase locking (0.55). High frequencies increase the number of spikes in the out-of-phase NL cell. These are mistakes that arise by an insufficient phase locking. As is pointed out in Monsivais et al. (1996), the jitter in the phase locking leads to timing errors that confuse the coincidence detection in the NL cell. This is either because spikes in an out-of-phase cell arrive at the same time from both sides, by mistake, or because spikes in one side of the out-of-phase cell get summated postsynaptically (a.k.a. unilateral summation).

Agmon-Snir et al. (1998) suggested that the NL cells were one of few cases known where the dendrites actually played a major role in neural processing. While two spikes that arrive simultaneously to both dendrites are then summated linearly in the soma, two spikes that arrive simultaneously to the same dendrite are summated sublinearly. Thus, spikes that are unilaterally summated are shorter and they are recognizable from the spikes that mark the coincidence detection. This mechanism was shown in the CD model in Simon et al. (2001b).

However, Reyes et al. (1996) weighed the possibility that the inhibitory input may be a key factor in this process. An inhibitory contribution would help the cell distinguish between both cases. Nonetheless, they argued that, following a model of coincidence detection in MSO by Colburn et al. (1990) (see also Han and Colburn (1993)), inhibition might not be critically necessary. Bruckner and Hyson (1998) added that, without recording any inhibitory PSP, NL cells were able to distinguish between unilateral summation and binaural coincidence.

This idea was challenged by a model of the MSO of Reed and Durbeck (1995) that evidenced that a gain control mechanism was necessary. Their argument was that since MSO neurons saturate with a high input, out-of-phase neurons would match eventually the output of a saturated in-phase cell. Thus, the inhibition would play a role, but only in certain cases. Pena et al. (1996) showed how this model could work in NL. Our experiments show also that an analogous rationale may work with regard to frequency response. As we have seen, the best improvement in discrimination in the NL cell comes in the case of high frequency (2000 Hz) and rather good phase locking (0.55). We can observe that out-of-phase spikes decrease quicker than in-phase spikes, compensating somehow the effect of unilateral summation and boosting the discrimination.

#### Assessment of the input of the SON.

The next set of experiments is devised to analyze the nature of the input to the SON. Our objective is to characterize the NA and NL input and to calibrate how should it be to create tonic spiking in the SON.

The first experiment of the set consists in exciting the NL cell with different sounds and looking to the impact in the SON cell.

Frequency=700 Hz	$g_{\max}=0.08 \text{ } \mu\text{S}$	$\tau=0.1111 \text{ ms}$	VS as in owl
------------------	--------------------------------------	--------------------------	--------------

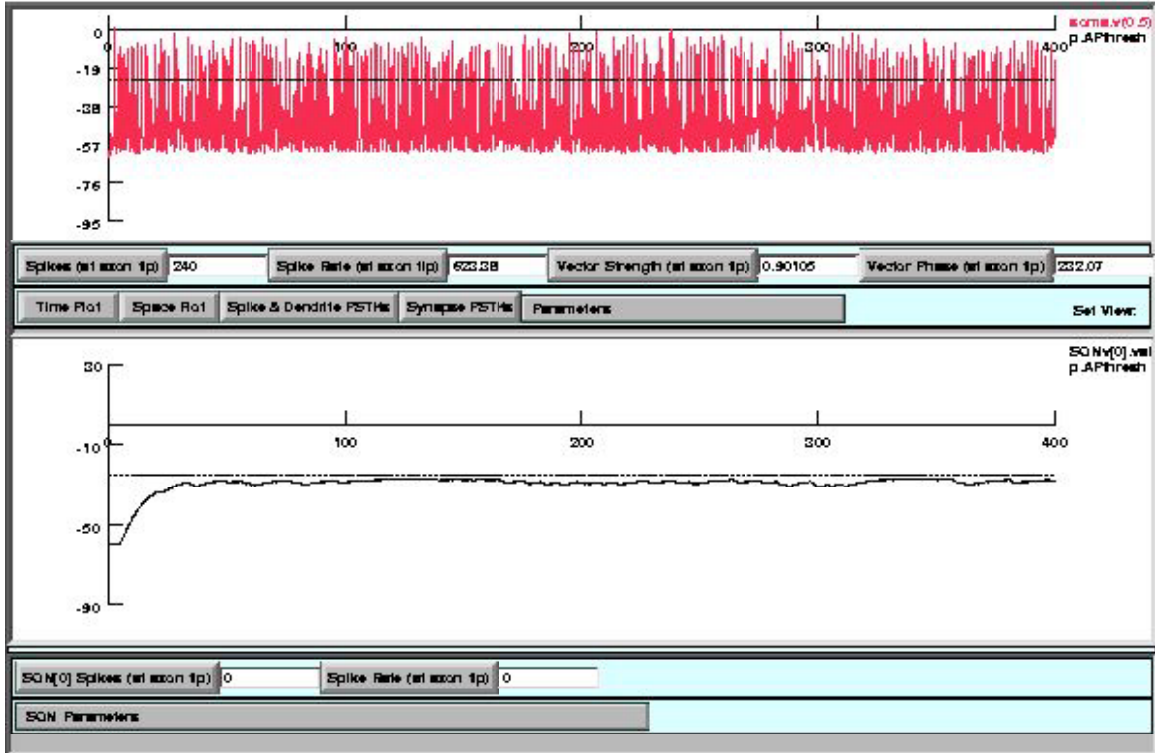


Figure 24. Effect in a SON cell of a NL cell spiking with a sound of 700 Hz.

As can be noticed in the simulation the threshold for spike activation in the SON cell is very high and by the time the voltage reaches it the conductance in the cell is so high that the sodium channels cannot be activated. On the other hand, the number of inputs is so big that the voltage is unable to decay and allow a posterior activation of the sodium channels.

The next experiment tries to test if a lower spiking rate allows the voltage in the SON cell to decay, which would help the creation of spikes activating the sodium channels.

Frequency=2000Hz	$g_{\max}=0.01 \text{ } \mu\text{S}$	$\tau=0.1111 \text{ ms}$	VS as in owl
------------------	--------------------------------------	--------------------------	--------------

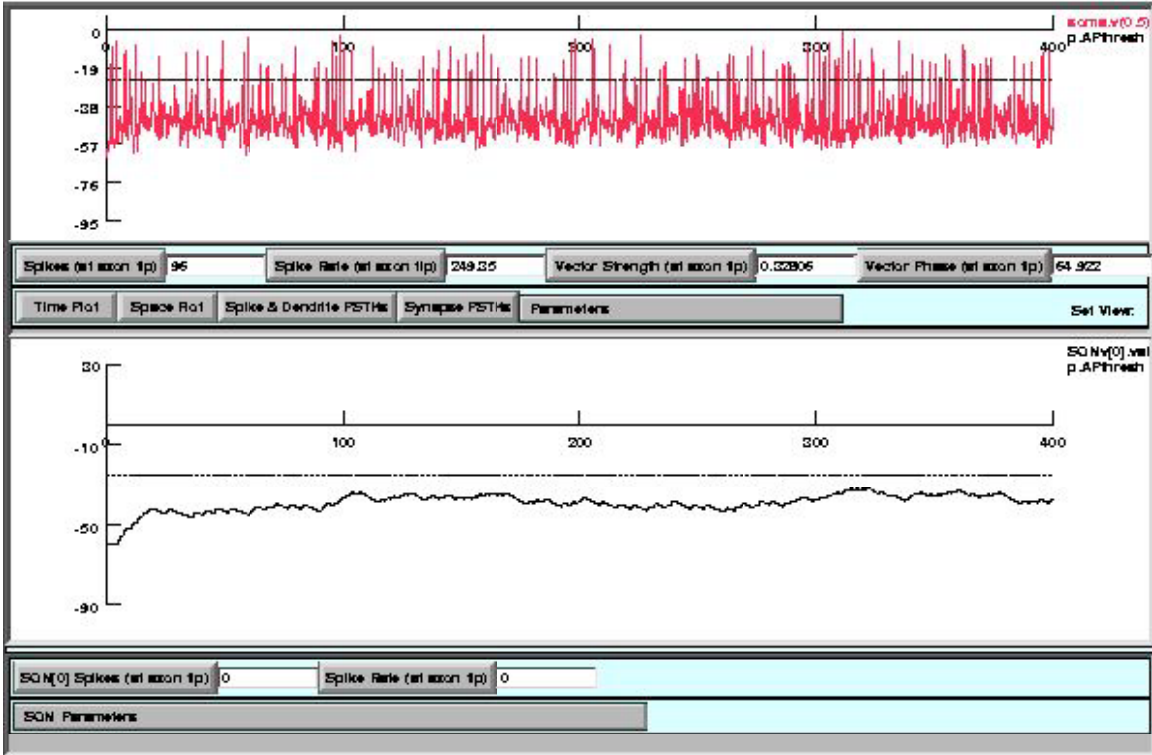


Figure 25. Effect in a SON cell of a NL cell spiking with a sound of 2000 Hz.

Bursts of spikes in the NL cell seem to almost trigger a spike in the SON cell. However, the input from NL is still too weak and slow in its rising to trigger a spike.

Trying with a variety of simulated inputs coming from NA, the next simulation pictures how spikes can get triggered.

NA prob. rate=0.05 (ms <sup>-1</sup> )	$g_{\max}(\text{NA})=0.15 \mu\text{S}$	NA syn. per SON dend=1
----------------------------------------	----------------------------------------	------------------------

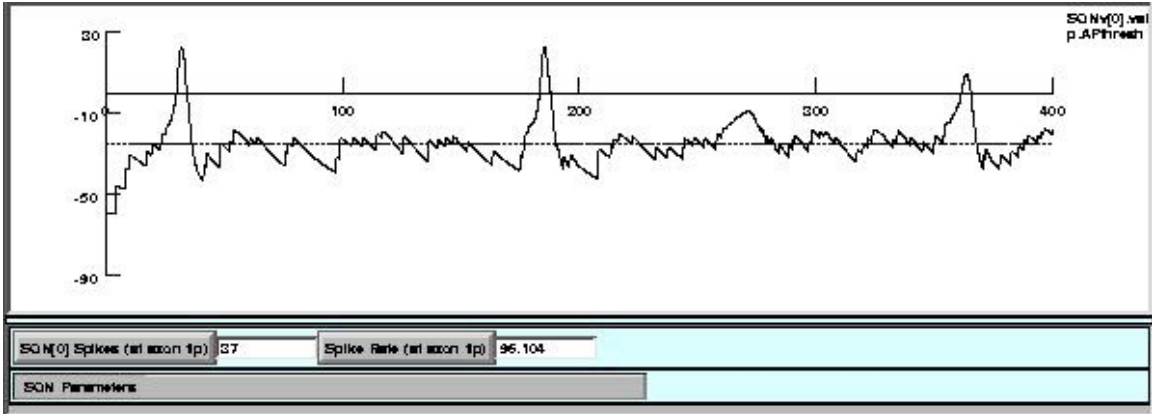


Figure 26. SON cell spiking fast (96 spikes/s) due to the input of the NA.

The probability rate of the NA input entails an average firing rate that is equal to its inverse,  $SR=1/0.05=20$  spikes/s. There is 1 synapse from NA in each SON dendrite.

In this experiment we can appreciate that in order to achieve a sustained spiking rate the SON cell needs an input of strong peak and very low frequency.

The next simulations are designed to test is the input from NL helps the input from NA in the spike triggering.

NA prob. rate= $0.05 \text{ (ms}^{-1}\text{)}$	$g_{\max}(\text{NA})=0.15 \text{ } \square\text{S}$	NA syn. per SON dend=1
Frequency=700 Hz	$g_{\max}=0.08 \text{ } \square\text{S}$	$\tau=0.1111 \text{ ms}$
		VS as in owl

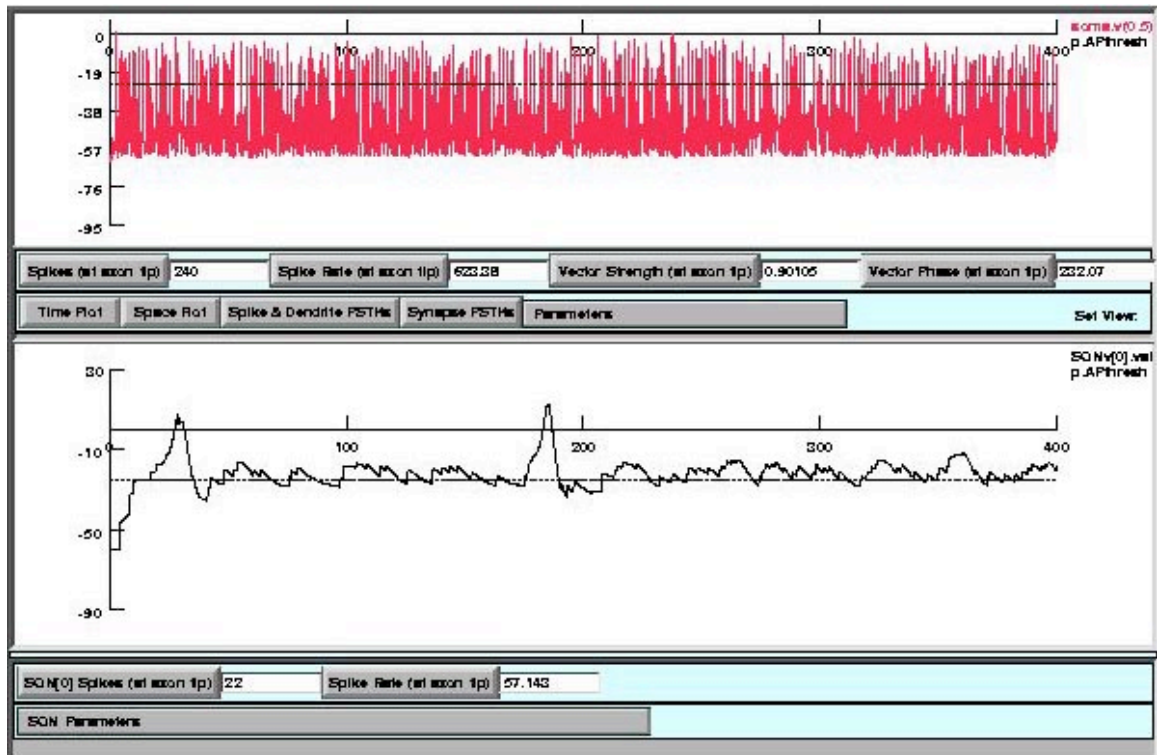


Figure 27. SON cell with a combined input from NA and a NL cell.

The NL cell input to the SON cell hinders the apparition of spikes, and the stronger is this input the more it hinders. It seems clear to us that the NL cell input is not capable of crossing the threshold of spike triggering quickly enough and then dwindle. The most notable impediment is this threshold, and it is so because the cell saturates at similar voltages as the threshold voltage. Looking to Yang et al. (1999) data it grabs our attention that the spiking threshold is much lower than the one we are using - about 25 mV lower. This is quite surprising, since Macleod's recordings and Yang et al. (1999) recordings seem to agree in characteristics such as the spiking rate, the spike shape or the resting potential.

A lower threshold would make it easier for the NL input to trigger spikes. The disagreement in this matter is important. We recall here that initial descriptions of SON

cells distinguish between at least two types of cells: ones that respond to bilateral input and others that respond to unilateral inputs (Takahashi and Konishi, 1988; Lachica et al., 1994). Our results contradict the homogeneity of the SON cells postulated by Yang et al. (1999). Differences in cell shape and threshold voltage would lead to a specialization in binaural or monoaural input. A more thorough physiological study of the SON cells could solve this problem.

Appendix A  
Rall assumptions  
(Rall, 1959).

1. A dendritic tree is assumed to consist of a cylindrical trunk and cylindrical branch components.
2. The electrical properties of the membrane are assumed to be uniform over the entire soma-dendritic surface, alternative assumptions are possible, but this assumption centers attention on the geometric aspects of the problem.
3. The electric potential is assumed to be constant over the entire external surface of the neuron. This is equivalent to assuming infinite conductivity of the external medium; such an assumption is commonly made for axons placed in a large volume of conducting medium. The use of this assumption can be shown to cause negligible error in the results. Briefly, this is because the gradients of electrical potential to be expected in an external medium of large volume, and of reasonable conductivity, are very much smaller than the corresponding internal (axial) gradients of potential.
4. The electric potential is assumed to be constant over the internal surface of the soma membrane. Together with assumption 3, this implies a uniform soma membrane potential. In this formal model, therefore, the shape of the soma surface is irrelevant, because the entire soma membrane is effectively a lumped membrane impedance. Thus lumped impedance represents the common point of origin for all dendritic trunks belonging to a single neuron. Strict validity of this assumption, during flow of current into the dendrites from an electrode place within the soma, would imply infinite conductivity within the soma.

5. The internal potential and current are assumed to be continuous at all dendritic branch points and at the soma-dendritic junction. This is an obvious physical requirement which merits explicit statement because of its importance in the mathematical treatment.
6. The electric current inside any cylindrical component is assumed to flow axially through an ohmic resistance which is inversely proportional to the area of the cross section.
7. The electric current across the membrane is assumed to be normal to the membrane surface. The uniformly distributed membrane impedance is assumed to consist of an ohmic resistance in parallel with a perfect capacity.
8. A membrane electromotive force,  $E$ , is assumed to be in series with the membrane resistance, and is assumed to be constant for all of the membrane. Under steady conditions, and in the absence of current flow, the electric potential difference,  $V_m$ , across the membrane has a resting value equal to  $E$ .

Appendix B  
Table of parameters

Array parameters

Cells per array	1 array
-----------------	---------

NA stimulus

Stimulus vector strength	0
Probability rate	0.05
# syn/dendrite	1 syn/dendrite
Center	0.5
Distribution	1
$\tau$	0.1 ms
$g_{max}$	0.005 $\mu$ S
$V_{rest}$	-10 mV
Duration	1 ms

CD to SON synapses

# syn./dendrite	1 syn./dendrite
Center	0.5
Distribution	1
Delay	2.6 ms
$\tau$	0.45 ms
$g_{max}$	0.009 $\mu$ S
$V_{rest}$	-10 mV
Duration	1 ms

SON to CD synapses

# syn. threshold	-25 mV
Center	0.5
Distribution	1
Delay	9.5 ms
$\tau_1$	4 ms
$\tau_2$	60 ms
$g_{max}$	0.006 $\mu$ S
$V_{rest}$	-34 mV
Syn. threshold	-15 mV

Dendrites

# dendrites	6 dendrites
Length	120 $\mu$ m
Diameter	4.8 $\mu$ m
Axial resistance	200 $\Omega$ *cm
$g_{Leak}$	$1.637 \cdot 10^{-5}$ S/cm <sup>2</sup>
# compartments	10 compartments

Soma

Length	18 $\mu$ m
--------	------------

Diameter	18 $\mu$ m
Axial resistance	200 $\Omega$ *cm
$g_{Leak}$	0.0006286 S/cm <sup>2</sup>
$g_{Na}$	0.078 S/cm <sup>2</sup>
$g_K$	0.075 S/cm <sup>2</sup>
# compartments	1 compartment

Axon

Length	40 $\mu$ m
Diameter	4.8 $\mu$ m
Axial resistance	200 $\Omega$ *cm
$g_{Leak}$	1.637*10 <sup>-5</sup> S/cm <sup>2</sup>
$g_{Na}$	0.078 S/cm <sup>2</sup>
$g_K$	0.075 S/cm <sup>2</sup>
# compartments	1 compartment

General parameters

$V_{Na}$	40 mV
$V_K$	-60 mV
$V_{Leak}$	-59 mV
$\tau_{0K}$	0.009 ms <sup>-1</sup>
$V_{HalfK}$	-20 mV
$V_{KK}$	10 mV
$\tau_{0K}$	0.025 ms <sup>-1</sup>
$V_{HalfK}$	-30 mV
$V_{KK}$	80 mV
$q_{10K}$	3
$T_{0K}$	23 °C
$\tau_{m0Na}$	0.03 ms <sup>-1</sup>
$V_{mVHalfNa}$	-5 mV
$V_{mKNa}$	10 mV
$\tau_{m0Na}$	0.108 ms <sup>-1</sup>
$V_{mVHalfNa}$	-30 mV
$V_{mKNa}$	18 mV
$\tau_{h0Na}$	0.0021 ms <sup>-1</sup>
$V_{hVHalfNa}$	-30 mV
$V_{hKNa}$	20 mV
$\tau_{h0Na}$	0.0175 ms <sup>-1</sup>
$V_{hVHalfNa}$	0 mV
$V_{hKNa}$	10 mV
$q_{10Na}$	3

Table 3. Parameters of the SON model.

Cells per Array (SON) (arrays)   1 Stimulus Vector Strength ((0->1))   0 Probability Rate (ms <sup>-1</sup> )   0.55 # [NA] (syn/dend)   1 Center [NA] ((0->1))   0.5 Distribution [NA] ((0->1))   1 tau [NA] (ms)   0.1 gmax [NA] (uS)   0.005 e [NA] (mV)   -10 Duration [NA] (ms)   1 # [CIS] (syn/dend)   1 Center [CIS] ((0->1))   0.5 Distribution [CIS] ((0->1))   1 Delay [CIS] (ms)   2.5 tau [CIS] (ms)   0.45 gmax [CIS] (uS)   0.009 e [CIS] (mV)   -10 Duration [CIS] (ms)   1 Syn Thresh [CIS] (mV)   -2.5 Center [SIC] ((0->1))   0.5 Distribution [SIC] ((0->1))   1 Delay [SIC] (ms)   9.5 tau1 [SIC] (ms)   4 tau2 [SIC] (ms)   60 gmax [SIC] (uS)   0.006 e [SIC] (mV)   -34 Syn Thresh [SIC] (mV)   -1.5	# [Den] (dendites)   6 Length [Den] (um)   120 Diameter [Den] (um)   4.8 Ax. Resist. [Den] (ohm cm)   200 gL [Den] (S/cm <sup>2</sup> )   1.537e-05 # Compartments [Den]   10 lambda [Den] (um)   873.38 Length [Soma] (um)   18 Diameter [Soma] (um)   18 Ax. Resist. [Soma] (ohm cm)   200 gLeak [Soma] (S/cm <sup>2</sup> )   0.0005295 gNa_m [Soma] (S/cm <sup>2</sup> )   0.078 gK_m [Soma] (S/cm <sup>2</sup> )   0.075 # Compartments [Soma]   1 Length [Axon] (um)   40 Diameter [Axon] (um)   4.8 Ax. Resist. [Axon] (ohm cm)   200 gLeak [Axon] (S/cm <sup>2</sup> )   1.537e-05 gNa_m [Axon] (S/cm <sup>2</sup> )   0.078 gK_m [Axon] (S/cm <sup>2</sup> )   0.075 # Compartments [Axon]   1 Current amplitude (nA)   0 Current Delay (ms)   0.1 Current Duration (ms)   400	eNa (mV)   40 eK (mV)   -60 eLeak (mV)   -59 alpha0 K (ms <sup>-1</sup> )   0.009 alphaVHalf K (mV)   -20 alphaK K (mV)   10 beta0 K (ms <sup>-1</sup> )   0.025 betaVHalf K (mV)   -30 betaK K (mV)   80 q10 K   3 T0 K   23 alpha0 Na (ms <sup>-1</sup> )   0.03 alphaVHalf Na (mV)   -5 alphaK Na (mV)   10 beta0 Na (ms <sup>-1</sup> )   0.108 betaVHalf Na (mV)   -30 betaK Na (mV)   18 alpha0 Na (ms <sup>-1</sup> )   0.0021 alphaVHalf Na (mV)   -30 alphaK Na (mV)   20 beta0 Na (ms <sup>-1</sup> )   0.0175 betaVHalf Na (mV)   0 betaK Na (mV)   10 q10 Na   3
------------------------------------------------------------------------------------------------------------------------------------------------------------------------------------------------------------------------------------------------------------------------------------------------------------------------------------------------------------------------------------------------------------------------------------------------------------------------------------------------------------------------------------------------------------------------------------------------------------------------------------------------------------------------------------------------------------------------------------------------------------------------------------------------------------	--------------------------------------------------------------------------------------------------------------------------------------------------------------------------------------------------------------------------------------------------------------------------------------------------------------------------------------------------------------------------------------------------------------------------------------------------------------------------------------------------------------------------------------------------------------------------------------------------------------------------------------------------------------------------------------------------------------------------------------------------------------------------------------------------------------------------------------------------------------	---------------------------------------------------------------------------------------------------------------------------------------------------------------------------------------------------------------------------------------------------------------------------------------------------------------------------------------------------------------------------------------------------------------------------------------------------------------------------------------------------------------------------------------------------------------------------------------------------------------------------------------------------

Figure 28. Panel of parameters of the SON model.

## BIBLIOGRAPHY

- Agmon-Snir H, Carr CE, Rinzel J. The role of dendrites in auditory coincidence detection. *Nature*. 1998 May 21;393(6682):268-72.
- Banks MI, Sachs MB. Regularity analysis in a compartmental model of chopper units in the anteroventral cochlear nucleus. *J Neurophysiol*. 1991 Mar;65(3):606-29.
- Boord RL. The anatomy of the avian auditory system. *Ann NY Acad Sci*. 1969;167:147-155.
- Brand A, Behrend O, Marquardt T, McAlpine D, Grothe B. Precise inhibition is essential for microsecond interaural time difference coding. *Nature*. 2002 May 30;417(6888):543-7.
- Bruckner S, Hyson RL. Effect of GABA on the processing of interaural time differences in nucleus laminaris neurons in the chick. *Eur J Neurosci*. 1998 Nov;10(11):3438-50.
- Carew TJ. Prey location in barn owls. In: *Behavioral Neurobiology*. Sunderland, Mass: Sinauer Associates; 2000.
- Carnevale NT, Hines ML. NEURON. 1999. Available at: <http://www.neuron.yale.edu>. Accessed July 10, 2002.
- Carr CE, Boudreau RE. An axon with a myelinated initial segment in the bird auditory system. *Brain Res*. 1993 Nov 19;628(1-2):330-4.
- Carr CE, Fujita I, Konishi M. Distribution of GABAergic neurons and terminals in the auditory system of the barn owl. *J Comp Neurol*. 1989 Aug 8;286(2):190-207.
- Carr CE, Konishi M. Axonal delay lines for time measurement in the owl's brainstem. *Proc Natl Acad Sci USA*. 1988 Nov;85(21):8311-5.
- Carr CE, Konishi M. A circuit for detection of interaural time differences in the brain stem of the barn owl. *J Neurosci*. 1990 Oct;10(10):3227-46.
- Chebib M, Johnston GA. The 'ABC' of GABA receptors: a brief review. *Clin Exp Pharmacol Physiol*. 1999 Nov;26(11):937-40. Review.
- Code RA, Burd GD, Rubel EW. Development of GABA immunoreactivity in brainstem auditory nuclei of the chick: ontogeny of gradients in terminal staining. *J Comp Neurol*. 1989 Jun 22;284(4):504-18.
- Colburn HS, Han YA, Culotta CP. Coincidence model of MSO responses. *Hear Res*. 1990 Nov;49(1-3):335-46.

- Conlee JW, Parks TN. Origin of ascending auditory projections to the nucleus mesencephalicus lateralis pars dorsalis in the chicken. *Brain Res.* 1986 Mar 5;367(1-2):96-113.
- Funabiki K, Koyano K, Ohmori H. The role of GABAergic inputs for coincidence detection in the neurones of nucleus laminaris of the chick. *J Physiol.* 1998 May 1;508 ( Pt 3):851-69.
- Goldberg JM, Brown PB. Response of binaural neurons of dog superior olivary complex to dichotic tonal stimuli: Some physiological mechanisms of sound localization. *J Neurophysiol.* 1969;32:613-636.
- Grothe B. The evolution of temporal processing in the medial superior olive, an auditory brainstem structure. *Prog Neurobiol.* 2000 Aug;61(6):581-610. Review.
- Han Y, Colburn HS. Point-neuron model for binaural interaction in MSO. *Hear Res.* 1993 Jun;68(1):115-30.
- Hines ML, Carnevale NT. The NEURON simulation environment. *Neural Comput.* 1997;9:1179-1209.
- Hodgkin AL, Huxley AF. A quantitative description of membrane current and its application to conduction and excitation in nerve. *J Physiol.* 1952;117:500-544.
- Hodgkin AL, Huxley AF, Katz B. Measurement of current-voltage relations in the membrane of the giant axon of *Loligo*. *J Physiol.* 1952;116:424-448.
- Hyson RL, Overholt EM, Lippe WR. Cochlear microphonic measurements of interaural time differences in the chick. *Hear Res.* 1994 Dec;81(1-2):109-18.
- Hyson RL, Reyes AD, Rubel EW. A depolarizing inhibitory response to GABA in brainstem auditory neurons of the chick. *Brain Res.* 1995 Apr 17;677(1):117-26.
- Hyson RL, Sadler KA. Differences in expression of GABA<sub>A</sub> receptor subunits, but not benzodiazepine binding, in the chick brainstem auditory system. *J Mol Neurosci.* 1997 Jun;8(3):193-205.
- Jeffress LA. A place theory of sound localization. *J Comp Physiol Psychol.* 1948;41:35-39.
- Johnston D, Wu SM. *Foundations of cellular neurophysiology*. Cambridge, Mass: MIT Press; 1995.
- Kandel ER, Schwartz JH. *Principles of Neural Science*. New York: Elsevier Science; 1985.
- Koppl C. Tonotopic projections of the auditory nerve to the cochlear nucleus angularis in the barn owl. *J Assoc Res Otolaryngol.* 2001 Mar;2(1):41-53.

- Koyano K, Funabiki K, Ohmori H. Voltage-gated ionic currents and their roles in timing coding in auditory neurons of the nucleus magnocellularis of the chick. *Neurosci Res.* 1996 Sep;26(1):29-45.
- Kubke MF, Carr CE. Development of the auditory brainstem of birds: comparison between barn owls and chickens. *Hear Res.* 2000 Sep;147(1-2):1-20. Review.
- Lachica EA, Rubsamén R, Rubel EW. GABAergic terminals in nucleus magnocellularis and laminaris originate from the superior olivary nucleus. *J Comp Neurol.* 1994 Oct 15;348(3):403-18.
- Lu T, Trussell LO. Inhibitory transmission mediated by asynchronous transmitter release. *Neuron.* 2000 Jun;26(3):683-94.
- Lu T, Trussell LO. Mixed excitatory and inhibitory GABA-mediated transmission in chick cochlear nucleus. *J Physiol.* 2001 Aug 15;535(Pt 1):125-31.
- Martin KE. NEURON programming tutorial. 2000 Nov 6. Available at: <http://www.neuron.yale.edu/neuron/docs/tutorial/index.html>. Accessed July 10, 2002.
- Monsivais P, Rubel EW. Accommodation enhances depolarizing inhibition in central neurons. *J Neurosci.* 2001 Oct 1;21(19):7823-30.
- Monsivais P, Yang L, Rubel EW. GABAergic inhibition in nucleus magnocellularis: implications for phase locking in the avian auditory brainstem. *J Neurosci.* 2000 Apr 15;20(8):2954-63.
- Muller CM. gamma-Aminobutyric acid immunoreactivity in brainstem auditory nuclei of the chicken. *Neurosci Lett.* 1987 Jun 26;77(3):272-6.
- Overholt EM, Rubel EW, Hyson RL. A circuit for coding interaural time differences in the chick brainstem. *J Neurosci.* 1992 May;12(5):1698-708.
- Parameshwaran S, Carr CE, Perney TM. Expression of the Kv3.1 potassium channel in the avian auditory brainstem. *J Neurosci.* 2001 Jan 15;21(2):485-94.
- Parks TN, Rubel EW. Organization and development of brain stem auditory nuclei of the chicken: organization of projections from n. magnocellularis to n. laminaris. *J Comp Neurol.* 1975 Dec 15;164(4):435-48.
- Pena JL, Viète S, Albeck Y, Konishi M. Tolerance to sound intensity of binaural coincidence detection in the nucleus laminaris of the owl. *J Neurosci.* 1996 Nov 1;16(21):7046-54.
- Pena JL, Viète S, Funabiki K, Saberi K, Konishi M. Cochlear and neural delays for coincidence detection in owls. *J Neurosci.* 2001 Dec 1;21(23):9455-9.

- Rall W. Branching dendritic trees and motoneuron membrane resistivity. *Exptl Neurol.* 1959;1:491-527.
- Rall W. Membrane potential transients and membrane time constant of motoneurons. *Exptl Neurol.* 1960;2:503-532.
- Rall W. Theoretical significance of dendritic trees for neuronal input-output relations. In: Reiss RF, ed. *Neural theory and modeling*. Stanford Univ. Press; 1964.
- Rall W. *The theoretical foundation of dendritic function: selected papers of Wilfrid Rall with commentaries*. Segev I, Rinzel J, Sheperd GM, ed. Cambridge, Mass: MIT Press; 1995.
- Reed CR, Durbeck L. Delay lines and auditory processing. In: *Comments on modern biology*, Vol C, *Comments on theoretical biology*. London: Gordon and Breach; 1995: 441-461.
- Reyes AD, Rubel EW, Spain WJ. In vitro analysis of optimal stimuli for phase-locking and time-delayed modulation of firing in avian nucleus laminaris neurons. *J Neurosci.* 1996 Feb 1;16(3):993-1007.
- Rubel EW, Parks TN. Organization and development of brain stem auditory nuclei of the chicken: tonotopic organization of n. magnocellularis and n. laminaris. *J Comp Neurol.* 1975 Dec 15;164(4):411-33.
- Simon JZ, Carr CE, Shamma SA. A dendritic model of coincidence detection in the avian brainstem. *Neurocom.* 1999;26-27:263-269.
- Simon JZ, Parameshwaran S, Penney T, Carr CE. Temporal Coding in the Auditory Brainstem of the Barn Owl, Physiological and Psychophysical Bases of Auditory Function. In: Breebaart DJ, Houtsma AJM, Kohlrausch A, Prijs VF, Schoonhoven R, eds. *Physiological and Psychophysical Bases of Auditory Function*. Maastricht, NL: Shaker; 2001a.
- Simon JZ, Grau-Serrat V, Rodriguez-Esteban R, Carr CE. Biophysical model of coincidence detection in nucleus laminaris neurons. Society For Neuroscience. 2001b.
- Smith DJ, Rubel EW. Organization and development of brain stem auditory nuclei of the chicken: dendritic gradients in nucleus laminaris. *J Comp Neurol.* 1979 Jul 15;186(2):213-39.
- Soares D, Carr CE. The cytoarchitecture of the nucleus angularis of the barn owl (*Tyto alba*). *J Comp Neurol.* 2001 Jan 8;429(2):192-205.
- Soares D, Chitwood RA, Hyson RL, Carr CE. Intrinsic neuronal properties of the chick nucleus angularis. *J Neurophysiol.* 2002 Jul;88(1):152-62.

- Sullivan WE, Konishi M. Segregation of stimulus phase and intensity coding in the cochlear nucleus of the barn owl. *J Neurosci*. 1984 Jul;4(7):1787-99.
- Takahashi T, Moiseff A, Konishi M. Time and intensity cues are processed independently in the auditory system of the owl. *J Neurosci*. 1984 Jul;4(7):1781-6.
- Takahashi T, Konishi M. Projections of nucleus angularis and nucleus laminaris to the lateral lemniscal nuclear complex of the barn owl. *J Comp Neurol*. 1988 Aug 8;274(2):212-38.
- Viete S, Pena JL, Konishi M. Effects of interaural intensity difference on the processing of interaural time difference in the owl's nucleus laminaris. *J Neurosci*. 1997 Mar 1;17(5):1815-24.
- von Bartheld CS, Code RA, Rubel EW. GABAergic neurons in brainstem auditory nuclei of the chick: distribution, morphology, and connectivity. *J Comp Neurol*. 1989 Sep 22;287(4):470-83.
- Yang L, Monsivais P, Rubel EW. The superior olivary nucleus and its influence on nucleus laminaris: a source of inhibitory feedback for coincidence detection in the avian auditory brainstem. *J Neurosci*. 1999 Mar 15;19(6):2313-25.
- Yin TC, Chan JC. Interaural time sensitivity in medial superior olive of cat. *J Neurophysiol*. 1990 Aug;64(2):465-88.
- Young SR, Rubel EW. Frequency-specific projections of individual neurons in chick brainstem auditory nuclei. *J Neurosci*. 1983 Jul;3(7):1373-8.
- Young SR, Rubel EW. Embryogenesis of arborization pattern and topography of individual axons in nucleus laminaris of the chicken brain stem. *J Comp Neurol*. 1986;254:425-459.
- Warchol ME, Dallos P. Neural response to very low-frequency sound in the avian cochlear nucleus. *J Comp Physiol [A]*. 1989 Nov;166(1):83-95.
- Warchol ME, Dallos P. Neural coding in the chick cochlear nucleus. *J Comp Physiol [A]*. 1990 Mar;166(5):721-34.
- White JA, Young ED, Manis PB. The electrotonic structure of regular-spiking neurons in the ventral cochlear nucleus may determine their response properties. *J Neurophysiol*. 1994 May;71(5):1774-86.

